Nature Communications

https://doi.org/10.1038/s41467-026-69638-z

Article in Press

Tumor-associated CD19^{+} macrophages induce immunosuppressive microenvironment in hepatocellular carcinoma

Received: 22 March 2025

Accepted: 5 February 2026

Cite this article as: Wang, J., Cao, W., Huang, J. *et al.* Tumor-associated CD19^{+} macrophages induce immunosuppressive microenvironment in hepatocellular carcinoma. *Nat Commun* (2026). https://doi.org/10.1038/s41467-026-69638-z

Junli Wang, Wanyue Cao, Jinyan Huang, Yu Zhou, Rujia Zheng, Yu Lou, Jiaqi Yang, Jiawei Yan, Jianghui Tang, Mao Ye, Zhengtao Hong, Jiangchao Wu, Haonan Ding, Yuquan Zhang, Jianpeng Sheng, Xinjiang Lu, Pinglong Xu, Xiongbin Lu, Xueli Bai, Tingbo Liang & Qi Zhang

Tumor-associated CD19^{+} macrophages induce immunosuppressive microenvironment in hepatocellular carcinoma

Junli Wang[1,2,#], Wanyue Cao[1,2,#], Jinyan Huang[2,7], Yu Zhou[2], Rujia Zheng[2,7], Yu Lou[1,2], Jiaqi Yang[1,2], Jiawei Yan[1,2], Jianghui Tang[1,2], Mao Ye[1,2], Zhengtao Hong[1,2], Jiangchao Wu[1,2], Haonan Ding[1,2], Yuquan Zhang[1,2], Jianpeng Sheng[2,5,6], Xinjiang Lu[2,8], Pinglong Xu[2,5,9], Xiongbin Lu[1,2], Xueli Bai[1,2,3,4,5,6], Tingbo Liang[1,2,3,4,5,6,*], Qi Zhang[1,2,3,4,5,6,*]

[1] Department of Hepatobiliary and Pancreatic Surgery, the First Affiliated Hospital, Zhejiang University School of Medicine, Hangzhou 310003, China.

[2] Zhejiang Provincial Key Laboratory of Pancreatic Disease, the First Affiliated Hospital, Zhejiang University School of Medicine, Hangzhou 310003, China.

[3] Clinical Research Center of Hepatobiliary and Pancreatic Diseases, Zhejiang Province, Hangzhou 31003, China.

[4] The Innovation Center for the Study of Pancreatic Diseases of Zhejiang Province, Hangzhou 310003, China.

[5] Zhejiang University Cancer Center, Hangzhou 310063, China.

[6] MOE Joint International Research Laboratory of Pancreatic Diseases, Hangzhou 310003, China.

[7] Biomedical Big Data Center, the First Affiliated Hospital, Zhejiang University School of Medicine, Hangzhou 31003, China.

[8] Department of Physiology, Zhejiang University School of Medicine, Hangzhou 310063, China.

[9] Life Sciences Institute, Zhejiang University, Hangzhou 310063, China

[#] These authors contributed equally.

[*]Correspondence: qi.zhang@zju.edu.cn (Q.Z.); liangtingbo@zju.edu.cn (T.L.)

Abstract

Tumor-associated macrophages are a key component that contributes to the immunosuppressive microenvironment in human cancers. However, therapeutic targeting of macrophages has been a challenge in clinic due to the limited understanding of their heterogeneous subpopulations and distinct functions. Here, we identify a clinically relevant $CD19^+$ subpopulation of macrophages that is enriched in many types of cancer, particularly in hepatocellular carcinoma (HCC). The $CD19^+$ macrophages exhibit increased levels of programmed cell death 1 ligand 1 (PD-L1) and CD73, enhanced mitochondrial oxidation, and compromised phagocytosis, indicating their immunosuppressive functions. Targeting $CD19^+$ macrophages with anti-CD19 chimeric antigen receptor T (CAR-T) cells inhibited HCC tumor growth. We identify Paired Box 5 (PAX5) as a primary driver of up-regulated mitochondrial biogenesis in $CD19^+$ macrophages, which depletes cytoplasmic Ca^{2+}, leading to lysosomal deficiency and consequent accumulation of CD73 and PD-L1. Inhibiting CD73 or mitochondrial oxidation enhanced the efficacy of immune checkpoint blockade therapy in treating HCC, suggesting great promise for $CD19^+$ macrophage-targeting therapeutics.

Introduction

Liver cancer has emerged as the third leading cause of cancer-related death worldwide, with hepatocellular carcinoma (HCC) being the predominant pathological subtype[1]. Current therapies for treating HCC comprise surgical resection, liver transplantation, locoregional therapies, and systemic treatments including targeted therapies and immunotherapy[2]. Surgical resection and liver transplantation offer the best chance for a cure, but are only options for a small subset of patients diagnosed at an early stage. Locoregional therapies, including radiofrequency ablation and transarterial chemoembolization, are used for intermediate stages of HCC or when surgery is not feasible. Systemic treatments, like tyrosine kinase inhibitors (e.g., sorafenib and lenvatinib) and immune checkpoint inhibitors (e.g., atezolizumab, nivolumab and pembrolizumab),

have expanded treatment options for the majority of patients with advanced HCC that misses the window for surgical intervention[3]. Despite these advancements, the 5-year overall survival rates for HCC remain below 20%[4]. These therapies face significant challenges in the clinic, including tumor heterogeneity, which leads to variable treatment responses, and the immunosuppressive tumor microenvironment (TME), which hampers the efficacy of immunotherapies[5,6].

The immunosuppressive microenvironment of HCC is characterized by a complex interplay of various cell types that collectively inhibit effective anti-tumor immune responses. Key players include myeloid-derived suppressor cells (MDSCs), which accumulate and inhibit T cell activation[7]. Regulatory T cells (Tregs) suppress cytotoxic T cell function, while cancer-associated fibroblasts (CAFs) produce extracellular matrix components and cytokines that further support an immunosuppressive milieu[8]. Particularly, tumor-associated macrophages (TAMs) are the most abundant in HCC that promotes tumor growth and suppresses inflammation[9]. These various types of stroma cells interact through direct contact and the release of soluble factors, creating a TME that hinders immune-mediated tumor eradication[10].

Macrophages exhibit different features in the presence of different inducers, such as lipopolysaccharide and interleukin-4, which lead to the two classic polarizations of macrophages, defining as M1 and M2 macrophages[11]. TAMs are believed to promote tumor progression by reprogramming local immunosuppression, inducing angiogenesis and drug resistance, and promoting tumor cell invasion. Phenotypically, despite being considered to have an M2-like polarization[12], TAMs are noncanonical and dynamically altered in response to stimuli within the TME. Consequently, the binary classification of macrophages is inadequate for describing them within the highly heterogeneous TME, both spatially and temporally[13]. Studies have identified specific TAM subgroups, such as PD-1$^+$ TAMs in colon cancer, TREM1$^+$ TAMs in hepatocellular carcinoma, and CD169$^+$

TAMs in glioblastoma[14-16]. These subgroups have diverse or even contradictory effects on tumor progression, suggesting that precise interventions targeting certain TAM subgroups, rather than the wholesale removal of M1, M2 or all TAMs in the TME, are likely to achieve better anti-tumor efficacy. Therefore, understanding the full spectrum of TAMs is crucial for developing therapeutic approaches that target macrophages in HCC.

In the present study, we identified a subgroup of $CD19^+$ TAMs that are enriched in a number of solid tumor types, particularly in HCC. As a transmembrane glycoprotein, CD19 is considered as a biomarker and functionally crucial for the regulation of B cell receptor signaling in both the early and late stages of B cell development. Interestingly, a recent analysis of single-cell RNA sequencing (scRNA-seq) data defined a transdifferentiated cell types in the ischemic brain that was characterized by co-expression of B-cell markers and several macrophage markers[17], suggesting a potential role of CD19 in macrophages. Here, we elucidated the clinical relevance, cellular functions, and molecular features of $CD19^+$ TAMs and determined the underlying regulatory mechanisms of their immunosuppressive characteristics. Based on these findings, we propose that targeting $CD19^+$ TAMs or mitigating their pro-tumoral effects could be a promising strategy for treating HCC.

Results

CD19$^+$ macrophages are enriched in HCC

A group of tumor tissue samples (n = 30) from patients with HCC were analyzed with mass cytometry (CyTOF) for profiling their tumor immune microenvironment [6]. Unexpectedly, we identified a subgroup of TAMs expressing CD19 at a level comparable to that in B cells in the tumors (**Fig. 1A**). To validate the presence of CD19$^+$ TAMs, we further conducted immune profiling analysis of HCC samples in a 41-patient cohort. Approximately a half (29 out of 41) of the HCC samples had a considerable proportion (>20% of total TAMs) of CD19$^+$ TAMs. The existence of a CD19$^+$ subpopulation in the TAMs was further confirmed using immunofluorescence (**Fig. 1B**), ImageStream (**Fig. 1C and Supplementary Fig.1A**) and flow cytometry (**Fig. 1D and Supplementary Fig.1B**). Additionally, we applied multiplex immunohistochemical (mIHC) staining on tumors and their adjacent normal tissues using CD14, CD68, CD19, and CD20 markers to demonstrate CD19$^+$ TAMs at the single-cell level (**Fig. 1E**). Conventional macrophage markers, CD11b and CD68/CD14, were used to confirm their macrophage identity. Notably, the proportion of CD19$^+$ TAMs was much higher in HCC than in adjacent normal tissue or peripheral blood (**Fig. 1B and 1D**). In terms of cell size, the CD19$^+$ TAMs had greater FSC/SSC (forward scatter/side scatter) values in flow cytometry than those of B cells, suggesting their macrophage cell lineage rather than a B cell lineage (**Supplementary Fig.1C**).

Next, we wanted to determine whether CD19$^+$ TAMs exist in other types of solid tumors. In a total of six types of human solid tumors, including HCC, CD19$^+$ TAMs are enriched (**Fig. 1F**) compared with those in peripheral blood and normal tissues. In particular, HCC, renal carcinoma, colorectal cancer, pancreatic cancer, and gastric cancer had a median proportion of CD19$^+$ TAMs over 20% of total TAMs. Similarly, we detected CD19$^+$ macrophages in various normal tissues and peripheral blood in mice

(**Supplementary Fig.1D**). Moreover, the proportion of CD19$^+$ macrophages did not correlate with that of B cells in these tissues (**Supplementary Fig. 1E and 1F**), further suggesting that they are not derived from B cells. The results collectively suggest that CD19$^+$ macrophages naturally exist in the body but are enriched in solid tumors.

CD19$^+$ TAMs are associated with poor clinical outcomes in HCC

As no previous study reported this subgroup of TAMs, we wanted to examine the clinical relevance of CD19$^+$ macrophages in HCC. A human HCC tissue microarray was co-immunostained with anti-CD19 and anti-CD68 antibodies (**Supplementary Fig. 2A**). In a total of 191 tissue samples with valid co-immunostaining, we found that the abundance (shown as density) of CD19$^+$ TAMs was positively correlated with tumor size (**Supplementary Fig. 2B**) and tumor cell differentiation (**Supplementary Fig. 2C**), but not with disease stages (**Supplementary Fig. 2D**), suggesting CD19$^+$ TAMs may be recruited at early stage of tumor initiation for creating immunosuppressive TME. Importantly, HCC patients with greater density of CD19$^+$ TAMs had worse overall survival (hazard ratio 3.12, 95% confidential interval 1.23–7.89) and disease-free survival (**Fig. 2A and Supplementary Fig. 2E**). By contrast, the density of total TAMs had no correlation with overall survival of these patients (**Fig. 2B**). Consistent with its clinical relevance, the density of CD19$^+$ TAMs was positively correlated with tumor cell proliferation, as indicated by Ki-67 staining in human HCC samples (**Fig. 2C**). TME analysis of the HCC tissue microarray indicated that a high density of CD19$^+$ TAMs was associated with increased infiltration of Tregs but reduced infiltration of CD8$^+$ T cells (**Supplementary Fig. 2F**). Collectively, these results demonstrated that CD19$^+$ TAMs correlate with poor clinical prognosis in patients with HCC, underlying a potential modification of TME.

CD19$^+$ TAMs possess immunosuppressive abilities and promote HCC growth

To study the role of $CD19^+$ TAMs in shaping the TME, we further analyzed the CyTOF data from the 41 patients with HCC (the same cohort analyzed in **Fig. 1A**). $CD19^+$ TAMs represent a major subgroup of TAMs, accounting for approximately 30% of TAMs and 5% of $CD45^+$ cells in the tumors (**Supplementary Fig. 2G**). The $CD19^+$ and $CD19^-$ subsets of TAMs showed a sharp difference at the level of the M2 macrophage marker CD163 (**Supplementary Fig. 2H**). The proportion of $CD19^+$ TAMs was also negatively correlated with the abundance of total T, $CD4^+$ and $CD8^+$ T cells (**Supplementary Fig. 2I**). In-depth analysis showed that the proportion of $CD19^+$ TAMs was positively correlated with that of PD-1^+ effector memory T cells (TEMs), but negatively correlated with that of $CD127^+$ TEMs (**Supplementary Fig. 2I**). These data strongly suggest that $CD19^+$ TAMs possess immunosuppressive abilities.

To determine the role of $CD19^+$ macrophages in tumor growth in vivo, we isolated $CD19^+$ and $CD19^-$ macrophages from mouse spleen and mixed them with mouse HCC cells (Hepa 1-6) to generate orthotopic syngeneic mouse models (**Supplementary Fig. 3A**). The presence of $CD19^+$ macrophages significantly promoted tumor growth in comparison to $CD19^-$ macrophages (**Fig. 2D**). Meanwhile, the number of infiltrating $CD8^+$ T cells was much lower, but Gr-1+ cells were more abundant in tumors with $CD19^+$ macrophages (**Supplementary Fig. 3B and 3C**). To test the clinical potential of targeting $CD19^+$ macrophages in HCC, we developed mouse chimeric antigen receptor T (CAR-T) cells specifically targeting mouse CD19 (see details in **Supplementary Methods**) for adoptive T cell therapy (**Supplementary Fig. 3D**). The growth of the tumors with $CD19^+$ macrophages, but not with $CD19^-$ macrophages, was significantly inhibited when the tumor-bearing mice received anti-CD19 CAR-T cells. This inhibition was not observed in the mice treated with control CAR-T cells for tumors containing either $CD19^+$ or $CD19^-$ macrophages (**Fig. 2E and Supplementary Fig. 3E**). To exclude the possibility that the inhibition is associated with B cells that are also positive for CD19, we tested the anti-

tumor effect of the anti-CD19 CAR-T in *muMT* mice that lack mature B cells[18]. Low levels of B cells in *mu*MT mice were verified by flow cytometry (**Supplementary Fig. 3F**). GFP$^+$ anti-CD19 CAR-T cells were infiltrated into tumors in *muMT* mice (**Supplementary Fig. 3G**) and CD19$^+$ macrophages were effectively depleted by the anti-CD19 CAR-T treatment (**Supplementary Fig. 3H**) The similar anti-tumor effect of anti-CD19 CAR-T cells was observed in the tumors with CD19$^+$ macrophages (**Fig. 2F**), independent of the B cell levels in the mice. These results highlight the role of CD19$^+$ macrophages in HCC progression and suggested CD19$^+$ macrophages are a potential clinical target for HCC treatment.

CD19$^+$ TAMs exhibit a distinct gene expression profile

To understand the molecular features of CD19$^+$ macrophages, we isolated CD19$^+$ TAMs, CD19$^-$ TAMs and B cells from three HCC patients, and conducted scRNA-seq analysis for a total of 52,749 cells (**Fig. 3A and Supplementary Fig. 4A**). TAMs were annotated by a high expression level of *CD11b, CD14* and *CD68*, while B cells were identified by *CD45, CD19* and *CD79A.* CD19$^+$ TAMs, CD19$^-$ TAMs and B cells were clustered (**Fig. 3B**). We next characterized the transcriptional profiles of the three types of cells (**Fig. 3C**). CD19$^+$ TAMs exhibited a distinctive gene signature, among which ribonuclease 1 (*RNASE1)*, selenoprotein P (*SELENOP)* and apolipoprotein E *(APOE)* are closely associated with cell metabolism. CD19$^-$ TAMs expressed high levels of genes encoding small calcium-binding proteins in the S100 family including *S100A9*, *S100A8* and *S100A4*. Interestingly, CD19$^+$ TAMs and B cells both express high levels of genes (*IGHG1*, *IGLC1* and *IGKC*) encoding immunoglobin proteins. Furthermore, CD19$^+$ TAMs appeared to be in proximity to M2-like macrophages, while CD19$^-$ TAMs were close to M1 macrophages to some extent, although no definite associations were found (**Fig. 3D and Supplementary Fig. 4B**). Genes in metabolic pathways and lysosome were significantly enriched in CD19$^+$ TAMs

(**Fig. 3E**). Specifically, CD19$^+$ TAMs had higher expression levels of genes associated with mitochondrial functions and higher mitochondria scores (**Fig. 3F and 3G**). The gene expression profiling analysis demonstrated that CD19$^+$ macrophages are a subgroup of cells distinct from CD19$^-$ macrophages and B cells.

Based on the scRNA-seq data analysis, we identified a 10-gene signature capable of distinguishing between CD19$^+$ and CD19$^-$ macrophages. This signature includes five genes specific to CD19$^+$ TAMs (*RNASE1, APOE, APOA2, APOC1, SELENOP*) and five genes specific to CD19$^-$ TAMs (*S100A9, S100A8, S100A4, FCN1, VCAN*) (**Supplementary Fig. 4C**). The mRNA expression profiles of these 10 genes effectively differentiate CD19$^+$ TAMs from CD19$^-$ TAMs, aligning well with their protein levels determined by flow cytometry (**Supplementary Fig. 4D and 4E**). This 10-gene signature was also applied to analyze two public scRNA-seq datasets (Bioproject: PRJCA010606 and PRJCA007744) (**Supplementary Fig. 5A-5C and 6A-6C**). The defined CD19$^+$ TAMs are highly enriched in HCC compared to normal adjacent tissues and show a higher level of mitochondrial activity than CD19$^-$ TAMs (**Supplementary Fig. 5D, 5E and 6D, 6E**).

CD19$^+$ TAMs are highly proliferative and immunosuppressive

Given the high mitochondria score of CD19$^+$ TAMs in HCC, we next analyzed the metabolic activity of mitochondria based on the expression levels of oxidative phosphorylation (OXPHOS)-related genes, including NADH dehydrogenase members, cytochrome c oxidase subunit members, and ATP synthase membrane subunit members in CD19$^+$ TAMs and CD19$^-$ TAMs. Overall, a majority of these genes was significantly up-regulated in CD19$^+$ TAMs (**Fig. 4A**). To further characterize the metabolic phenotype of CD19$^+$ TAMs, we sorted CD19$^+$ and CD19$^-$ TAMs from human HCC tissues and subjected to mitochondrial mass staining and reactive oxygen species (ROS) staining. Results revealed that CD19$^+$ TAMs exhibit enhanced mitochondrial mass, accompanied

by increased ROS production relative to $CD19^-$ TAMs (**Supplementary Fig. 7A and 7B**). Moreover, we found that $CD19^+$ TAMs exhibit increased co-expression of COX-IV, a key subunit of mitochondrial complex IV, supporting the maintenance of robust OXPHOS activity in $CD19^+$ TAMs (**Supplementary Fig. 7C**). Seahorse analysis of cell metabolism showed remarkably enhanced mitochondrial respiration of $CD19^+$ macrophages, including both basal and maximal respiratory capacities (**Fig. 4B**). The energetic feature of $CD19^+$ macrophages may lead to the alterations of their functions and cell activities. First, $CD19^+$ TAMs showed much compromised phagocytotic activity (**Fig. 4C**). Second, we found that the proportion of $CD19^+$ TAMs was significantly higher in large tumors than in small ones in an HCC syngeneic mouse model (**Supplementary Fig. 7D**), consistent with their clinical relevance in human HCC. $CD19^+$ TAMs showed higher levels of Ki-67 expression than $CD19^-$ TAMs from the same tumor, both in mice and patients (**Supplementary Fig. 7E and 7F**). The enhanced proliferation of $CD19^+$ TAMs was confirmed using an orthotopic mouse model and 5-ethynyl-2′-deoxyuridine (EdU) assays (**Supplementary Fig. 7G**). Therefore, we reasoned that abundance of $CD19^+$ TAMs in tumors, especially large ones, is likely due to their high proliferation rate.

As $CD19^+$ TAMs are a biomarker for poor clinical outcomes of HCC, we found increased PD-L1 levels in $CD19^+$ TAMs compared to $CD19^-$ TAMs (**Fig. 4D**). During the HCC metabolite analysis[6], we were particularly interested in adenosine, a primary immunosuppressive metabolite presents in high levels in the TME of most solid tumors[19]. In the metabolite data from the analysis using liquid chromatography with tandem mass spectrometry (LC-MS/MS), we observed significant associations between the concentrations of adenosine diphosphate (ADP), adenosine monophosphate (AMP), and adenosine and the abundance of $CD19^+$ TAMs in human HCC tumors (**Supplementary Fig. 7H**). Factors that contribute to adenosine production include hypoxia, high cell turnover, and particularly, the expression of CD73, a 5′-nucleotidase (NT5E) that converts

autocrine and paracrine danger signals of ATP to anti-inflammatory adenosine[20]. Given its pivotal role in regulating the ADP/AMP/adenosine conversion[21], CD73 has been an emerging therapeutic target for immune checkpoint blockade[22, 23], and numerous CD73-targeted antibodies and small-molecule inhibitors are currently undergoing clinical testing for cancer therapy[24]. As expected, we observed significantly elevated levels of CD73 in $CD19^+$ TAMs (**Fig. 4D**). Biochemical assay verified a high 5′-nucleotidase activity of CD73 in the $CD19^+$ TAMs (**Fig. 4E**). As an indicator of their immunosuppressive functions, $CD19^+$ macrophages significantly inhibited the proliferation of total T cells, $CD4^+$ T cells, and $CD8^+$ T cells when these cells were isolated from the clinical tumor samples and co-cultured in vitro in mixed lymphocyte reaction (MLR) assays (**Fig. 4F**).

PAX5 is a master regulator for $CD19^+$ macrophages

CD19 is important for B cell development and differentiation[25]. Therefore, it is intriguing to determine whether CD19 expression is essential for the immunosuppressive activity of $CD19^+$ TAMs. To this end, *$CD19^{\triangle M\varphi}$* (*$CD19^{flox/flox}$;Lyz-Cre*) mice were generated to establish orthotopic mouse HCC tumor models with macrophage-specific knockout of CD19. Unexpectedly, no differences in orthotopic tumor growth were observed between *$CD19^{\triangle M\varphi}$* mice and their littermate controls (**Fig. 5A**), although CD19 expression was depleted in literally all the macrophages in the *$CD19^{\triangle M\varphi}$* mice (**Fig. 5B**). These results suggest that CD19 can only be used as a biomarker for the $CD19^+$ macrophages, but functionally dispensable for this subgroup of macrophages in the tumor. Among upstream regulators of CD19, PAX5 is the key transcription factor that governs the expression of CD19[26, 27]. We found that $CD19^+$ TAMs indeed had up-regulated expression of PAX5 at both mRNA and protein levels (**Fig. 5C-5E**). Thus, we reasoned that PAX5 may play a role in the $CD19^+$ macrophages. Exogenous overexpression of *PAX5* in human THP-1 cells (a model for macrophage-related cell activities) induced the expression of CD19, CD73 and PD-L1

(**Fig. 5F and 5G**). Similar results were observed in mouse immortalized bone marrow-derived macrophages (iBMDMs) (**Fig. 5H**). Functionally, overexpression of *PAX5* impaired phagocytosis in the mouse iBMDMs (**Supplementary Fig. 8A**). Collectively, PAX5 appears to be a master regulator for the essential features of $CD19^+$ macrophages in the tumor.

In the human THP-1 cells, overexpression of *PAX5* also profoundly enhanced mitochondrial respiration in terms of basal respiration, maximal respiration and ATP production (**Fig. 5I**). Electron microscopy analysis demonstrated that the number of mitochondria was much higher in the THP-1 cells with *PAX5* overexpression (**Fig. 5J**). The increased number of mitochondria and decreased mitochondrial superoxide levels were detected by flow cytometry in these cells (**Fig. 5K**). Importantly, PAX5 significantly enhanced the expression of PGC-1α, a potent inducer of mitochondrial biogenesis (**Supplementary Fig. 8B**)[28]. Additionally, *PAX5*-overexpressing THP-1 cells presented a higher level of adenosine in the culture medium than control cells, consistent with increased CD73 activity (**Supplementary Fig. 8C and 8D**). Since cellular metabolism is tightly related to macrophage functions[15], we asked whether regulation of mitochondrial metabolism affected CD73 activity in $CD19^+$ macrophages. Antimycin, an OXPHOS inhibitor, dramatically impaired CD73 activity (**Supplementary Fig. 8D**). Induction of reactive oxide species by diamide, rather than their removal by N-acetyl-cysteine (NAC), also inhibited CD73 activity. By contrast, blocking CD19 with neutralizing antibodies or inhibiting glycolysis with 2-deoxy-d-glucose (2-DG) had no effect on the CD73 activity (**Supplementary Fig. 8D**). Therefore, mitochondrial metabolism, but not CD19-associated cell signaling regulate the functions of $CD19^+$ macrophages in the tumor. Consistent with the cell studies, conditional knocked out of *Pax5* in mouse macrophages (*Pax5*$^{flox/flox}$*;Lyz-Cre*, named as *Pax5*$^{\triangle M\varphi}$) drastically inhibited the growth of orthotopically injected Hepa1-6-derived tumors (**Fig.5L and Supplementary Fig. 8E-8G**). As expected,

depletion of PAX5 efficiently decreased the protein levels of CD19, CD73, and PD-L1 in the macrophages of these mice (**Supplementary Fig. 8H**). Collectively, these results suggested that PAX5, instead of CD19, plays a central role in the regulation of $CD19^+$ macrophages in the tumor.

PAX5 induces PD-L1 and CD73 in a post-transcriptional manner

Interestingly, *PAX5* overexpression in human THP1 cells did not significantly induce the mRNA levels of *PD-L1* and *CD73* (**Fig. 6A**), indicating post-transcriptional regulation of PAX5 in $CD19^+$macrophages. We performed CUT&Tag (**C**leavage **U**nder **T**argets and **Tag**mentation) and RNA-seq assays on human THP-1 cells with or without *PAX5* overexpression and identified global expression changes of genes that are transcriptionally regulated by PAX5 (**Fig. 6B**). Among these changes, genes associated with lysosome pathways were the second most significantly enriched, behind the genes involved in phagocytosis (**Fig. 6C**), suggesting that PAX5 may control target protein degradation via lysosome. Heat shock cognate 71-kDa protein (HSC70) is a chaperon protein that brings target proteins to lysosomes for degradation in cells[29]. We first performed mIHC on human HCC samples, specifically quantifying the protein co-expression patterns of PAX5, HSC70, CD19, PD-L1, and CD73 within $CD19^+$TAMs. Results revealed that in $CD19^+$TAMs, PAX5 expression exhibited significant positive correlations with the expression of CD19, PD-L1, and CD73. However, no correlation was observed between PAX5 and HSC70 protein levels in these cells (**Supplementary Fig. 9A**). These findings suggested that PAX5 is proposed to influence HSC70-mediated protein degradation by altering these interaction dynamics rather than changes in the total abundance of HSC70. We then identified three KFERQ-like motifs (CMA), which are potential binding sites to HSC70, in both PD-L1 and CD73 (**Fig. 6D**). Coimmunoprecipitation assays validated protein interactions between HSC70 and PD-L1

or CD73 (**Fig. 6E**), While KFERQ-like motif mutations in PD-L1 and CD73 disrupted their interactions with HSC70 compared to the wild type (WT) proteins (**Supplementary Fig. 9B and 9C**). In lysosome function assays, we observed that lysosomes were significantly inhibited upon *PAX5* overexpression (**Fig. 6F and Supplementary 6G**). Meanwhile, both CD73 and PD-L1 were induced when *PAX5*-overexpresing THP-1 cells were treated with inhibitors of lysosomal proteolysis (NH_4Cl and leupeptin) (**Fig. 6H**).

Because decreased number of lysosomes were seen in the *PAX5*-overexpressing THP-1 cells, we speculated that PAX5 may also regulate the activity of TFEB (Transcription Factor EB), a master regulator of lysosomal biogenesis (**Supplementary Fig. 10A**)[30], in the nucleus. We found that nuclear TFEB levels were dramatically diminished in *PAX5*-overexpressing cells (**Fig. 6I and Supplementary Fig. 10B**). Knockdown of TFEB inhibited lysosomal functions and increased PD-L1 and CD73 protein levels, similar to the effects of *PAX5* overexpression (**Supplementary Fig.10C-10E**). Overexpression of TFEB offset the effects of *PAX5* overexpression, leading to reduced levels of PD-L1 and CD73 in the *PAX5*-overexpressing cells (**Supplementary Fig. 10F and 10G**). We sought to delineate the mechanism by which PAX5 regulates the nuclear translocation of TFEB. TFEB subcellular translocation is regulated primarily by Ca^{2+} signaling or mTOR-mediated phosphorylation[31,32]. While no change in mTOR expression was observed in the *PAX5*-overexpressing cells (data not shown), we reasoned that increasing calcium uptake by mitochondria, due to their up-regulated biogenesis in $CD19^+$ TAMs, may impact Ca^{2+} signaling in the cytosol[32]. Using a fluorescent probe, we found an increased level of mitochondrial Ca^{2+} and, accordingly, a decreased level of cytosolic Ca^{2+} in *PAX5*-overexpressing THP-1 cells (**Fig. 6J**). Treatment with IACS-010759 (an OXPHOS inhibitor) or ionomycin (a Ca^{2+} ionophore) significantly increased the cytosolic level of Ca^{2+} and thus promoted the nuclear level of TFEB (**Supplementary Fig. 10H and 10I**). These results suggested that PAX5 modulates the Ca^{2+} shuttling between

mitochondria and the cytosol, consequently inhibiting the nuclear translocation of TFEB and lysosomal activity, which eventually increases the levels of CD73 and PD-L1 by inhibiting their lysosomal degradation.

Blocking CD19$^+$ TAMs enhances the efficacy of immune checkpoint blockade therapy

Given the role of CD19$^+$ TAMs in HCC progression, we wanted to determine whether they could be a therapeutic target in treating HCC. In a syngeneic HCC tumor model, we first depleted macrophages in mice using clodronate liposomes every other day for four doses (**Supplementary Fig. 11A-11C**) prior to mouse Hepa1-6-derived tumor models establishment **(Supplementary Fig. 11D)**[33,34]. Control or *Pax5*-overexpressing iBMDMs were then infused into these mice to test their effects on tumor growth (**Supplementary Fig. 11D**). As expected, *Pax5*-overexpressing iBMDMs promoted greater tumor growth than wild-type iBMDMs (**Supplementary Fig. 11E**). In another orthotopic mouse model without systemic depletion of macrophages, *Pax5*-overexpressing iBMDMs also imposed a profound pro-tumor effect (**Fig. 7A**). Immunohistochemical analysis revealed that *Pax5*-overexpressing iBMDMs limited the tumor infiltration of CD8$^+$ T cells (**Fig. 7B**), indicating an immunosuppressive TME.

CD19$^+$ TAMs create an immunosuppressive tumor microenvironment with increased levels of PD-L1 and CD73. We next tested whether the combination of PD-L1 and CD73 blockade had a synergistic effect on tumor control (**Fig. 7C**). Anti-CD73 neutralizing antibodies or a small-molecule inhibitor of CD73 significantly enhanced the anti-tumor effect of anti-PD-L1 antibodies in an orthotopic HCC mouse model (**Fig. 7D**). These effects are solely dependent on PAX5 in the CD19$^+$ macrophages, as PD-L1 and CD73 blockade did not affect tumor progression in the *Pax5*$^{\triangle M\varphi}$ mice (**Supplementary Fig. 11F**). In the presence of anti-PD-L1 antibodies, CD73 blockade significantly increased the tumor

infiltration of $CD8^+$ T cells, as well as $CD4^+$ T cells and natural killer cells. Tumor cell proliferation was greatly suppressed, as indicated by reduced Ki-67 staining (**Supplementary Fig. 12**).

Because induced mitochondrial respiration is critical for the functions of $CD19^+$ TAMs, we tested whether inhibiting mitochondrial respiration of $CD19^+$ TAMs had a similar anti-tumor effect. The OXPHOS inhibitor IACS-010759 exhibited an improved anti-tumor effect when combined with anti-PD-L1 antibodies in the orthotopic mouse HCC tumor model (**Fig. 7E**). The combination of PD-L1 blockade and OXPHOS inhibition also significantly promoted tumor infiltration of immune cells, including CD4+ T cells and $CD8^+$ T cells (**Supplementary Fig. 13**). Collectively, therapeutic approaches targeting CD73 or OXPHOS -when optimized to leverage the heightened dependency of $CD19^+$ TAMs on these pathways show great promise for improving the anti-tumor efficacy of immunotherapy for HCC.

Discussion

TAMs play a crucial role in shaping the immunosuppressive tumor microenvironment. However, the heterogeneity of TAMs and the mechanisms by which they contribute to tumor progression remain elusive. In this study, we identified $CD19^+$ macrophages enriched in a number of human tumor tissues. A high density of $CD19^+$ macrophages within tumors is associated with poor clinical outcomes and reduced response to immunotherapy in patients with HCC. It was previously known that B cell progenitors, and even mature B cells, can be induced to adopt the gene expression patterns, morphology, and functions of macrophages[35]. Mechanistically, overexpression of transcription factor C/EBP in differentiated B cells leads to their rapid reprogramming into macrophages by inhibiting the B cell commitment transcription factor PAX5 and downregulation of its target CD19[35]. Extending this lineage plasticity, another prior study had demonstrated that cancers can induce the trans-differentiation of bone marrow-derived B-cell precursors—specifically $Csf1R^+Pax5^{Low}$ pre-B cells—into TAMs (termed B-MFs) via M-CSF signaling. A defining feature of B-MFs is the downregulation of PAX5 alongside the upregulation of macrophage-associated genes. Notably, these B-MFs are nearly absent in μMT mice[36]. Interestingly, $CD19^+$ macrophages retain high expression levels of PAX5 and CD19. Despite its essential role in B cell differentiation and signaling, CD19 itself appears to be dispensable for the pro-tumor functions of $CD19^+$ TAMs, at least in HCC. Depletion of CD19 in our preclinical mouse models had no notable effect on tumor growth (**Fig. 5A**). The abundance of $CD19^+$ macrophages was also not correlated with the numbers of B cells in the tissues (**Supplementary Fig. 1F**). In addition, cell morphology and size analysis suggest that $CD19^+$ TMAs is not likely to originate from a B cell lineage (**Fig. 1C and Supplementary Fig. 1C**). Further studies are warranted to determine whether $CD19^+$ TAMs are recruited from circulating non-resident macrophages or functionally switched from tissue-resident macrophages.

PAX5 is a deciding regulator for B-lineage commitment[37], and is usually undetectable in macrophages. However, PAX5 remains as a key player that drives immunosuppressive functions in the CD19$^+$ TAMs. *PAX5*-overexpressing macrophages phenocopied CD19$^+$ macrophages with all known characteristics, including enhanced oxidative phosphorylation, increased proliferative capacity, compromised phagocytic activity, and up-regulated levels of PD-L1 and CD73. However, CD19 does not seem to be transactivated in CD19$^+$ macrophages as it does in B cells. Instead, PAX5 induces the CD19 protein level in the macrophages by inhibiting its lysosomal degradation. This differential regulation may distinguish signaling networks between B cells and macrophages. It is now unclear how PAX5 is highly expressed in CD19$^+$ macrophages. This study is the first report showing a potential lineage crossing between B cells and macrophages in the tumor microenvironment. We observed varying levels of CD19$^+$ macrophages in the circulation and organs of both humans and mice, indicating the possible existence of these cells since embryonic development. This suggests that lineage restriction during hematopoietic stem cell differentiation may not be as stringent as previously thought, allowing for the generation of a small population of "hybrid cells."

CD19$^+$TAMs primarily promote HCC progression by maintaining an immunosuppressive tumor microenvironment enriched with Gr-1$^+$ cells. Gr-1$^+$ cells represent a heterogeneous population of immunosuppressive cells—encompassing neutrophils, myeloid-derived suppressor cells (MDSCs), and some monocyte subsets, their accumulation in tumors is strongly linked to poor clinical outcomes in cancer patients, including HCC[38,39]. In HCC, CD19$^+$TAMs and Gr-1$^+$ cells cooperated functionally to intensify the immunosuppressive state, thereby creating favorable conditions for tumor cell growth. However, whether CD19$^+$ TAMs orchestrate the recruitment of Gr-1$^+$ cells into the tumor microenvironment or, alternatively, Gr-1$^+$ cells mediate the recruitment of CD19$^+$ TAMs—has yet to be delineated. Currently, we are conducting mechanistic

experiments to clarify the cellular origin of CD19$^+$TAMs, as well as to investigate the infiltration dynamics of Gr-1$^+$cells. Future investigations are warranted to elucidat the crosstalk between these cell populations and advance the understanding of CD19$^+$TAMs biological characteristics in HCC.

CD19$^+$ TAMs are immunosuppressive due to their high levels of PD-L1 and CD73. CD73 expression in solid tumors has been identified as an independent biomarker of poor prognosis in clinic[40, 41]. Recent evidence has indicated that CD73 is selectively expressed in a diverse range of immune cell types, including T cells, natural killer cells, and macrophages[42]. The expression of CD73 on macrophages is closely associated with M2 polarization and resistance to anti-PD-1 antibodies[21, 43]. Our study demonstrated that PAX5 increases the levels of CD73 and PD-L1 by compromising lysosomal activity due to decreased nuclear translocation of TFEB in CD19$^+$ macrophages. The elevated activity of CD73 in these macrophages leads to increased adenosine production, which supports cancer cell proliferation in the tumor microenvironment. Given the hyperactivity of OXPHOS in CD19$^+$ TAMs, the combined inhibition of CD73 and OXPHOS, along with immune checkpoint blockade, presents a promising therapeutic approach for treating HCC and potentially other tumors enriched with CD19$^+$ TAMs.

In this study, we explored potential therapeutic strategies to deplete or inhibit CD19$^+$ TAMs, including CD19-targeted CAR-T cells, CD73 blockade, and OXPHOS inhibitors. CD19-targeted CAR-T therapies have consistently demonstrated high antitumor efficacy in both pediatric and adult patients with relapsed B-cell acute lymphoblastic leukemia, chronic lymphocytic leukemia, and B-cell non-Hodgkin lymphoma[44]. However, their clinical application in non-hematologic solid tumors remains to be established[45, 46]. Our results from a preclinical HCC model indicate significant translational potential for CD19-targeted CAR-T therapy in treating solid tumors with high levels of CD19$^+$ TAMs. CD73 blockade has demonstrated antitumor effects in preclinical experiments by eliciting

an effective immune response, including enhanced NK cell activity, improved CD4+ and CD8+ T cell function, and elevated levels of proinflammatory cytokines[22]. Beyond macrophages, CD73 expression on tumor cells and Tregs also suppresses antitumor immunity[21]. Thus, targeting CD73 may exert multifaceted effects in cancer treatment. Finally, OXPHOS inhibitors have become a focus in cancer therapeutics, enhancing treatment responses in various cancers, including melanomas, lymphomas, colorectal cancers, leukemias, and pancreatic ductal adenocarcinoma[47, 48]. However, the clinical efficacy of OXPHOS inhibitors is influenced by the complex TME. Our study suggests that OXPHOS inhibition may enhance clinical efficacy by targeting and suppressing $CD19^+$ TAMs in cancer immunotherapy.

In summary, we identified a subgroup of $CD19^+$ TAMs, which show immunosuppressive capacity and promoted HCC progression. Mechanistically, $CD19^+$ TAMs are primarily driven by PAX5 and have up-regulated PD-L1 and CD73 levels. Elimination of these macrophages by CD19-specific CAR-T cells or functional inhibition of them by inhibiting CD73 or OXPHOS sensitized HCC to immunotherapy.

Methods

Ethics Statement

All animal experiments were approved by the Ethics Committee of the First Affiliated Hospital, School of Medicine, Zhejiang University (approval number:No. 2020-483). The maximal permitted tumor size/burden as stipulated by this ethics committee is a single tumor diameter of no more than 20 mm, or a total tumor volume per animal of no more than 2000 mm^3; or tumor weight not exceeding 10% of the animal's body weight. All animals included in the study maintained tumor sizes/burdens within the permitted limits, and no instances of exceeding the maximal tumor size/burden were recorded.

The collection and application of clinical samples were approved by the ethics committee of the First Affiliated Hospital, Zhejiang University School of Medicine (approval number:No. 2020-681). All patients' informed consent was obtained.

A detailed description of the methods used in the study can be found in the **Supplementary information**.

Cell culture

THP-1 cells, Hepa1-6, Plat-E and HEK-293T cells were obtained from the American Type Culture Collection (ATCC, Manassas, VA), immortalized murine bone marrow-derived macrophages (iBMDMs) were provided by Jingying Zhang at Zhejiang University. THP-1 cells were cultured in Roswell Park Memorial Institute medium (RPMI 1640, Gibco, Carlsbad, CA). Hepa1-6, Plat-E and HEK-293T cells were cultured in high-glucose Dulbecco's modified Eagle's medium (DMEM, Gibco). Media were supplemented with 10% fetal bovine serum (FBS, Gibco) and 1% penicillin/streptomycin (Sigma-Aldrich, Saint Louis, MO), and maintained at 37.0 ± 0.2 °C in a humidified incubator with 5.0% CO2.

BMDMs were isolated from femurs and tibia of adult C57BL/6 mice (The Model Animal Research Center of Nanjing University, Nanjing, China) and cultured in RPMI 1640 medium containing 50 ng/ml recombinant murine macrophage colony-stimulating factor (M-CSF, Peprotech, Rocky Hill, NJ) for 5-day differentiation.

Mouse models

All mice were bred under pathogen-free conditions. Animal experiments were approved by the ethics committee of The First Affiliated Hospital, Zhejiang University School of Medicine. The maximal permitted tumour size/burden for the study was defined as a longest diameter of 20 mm or a tumour burden equivalent to 10% of the animal's body weight, in accordance with the ethical approval. Throughout the experimental period, none of the animals exceeded these predefined maximal tumour size or burden thresholds. Lyz-Cre mice were obtained from The Jackson Laboratory (Bar Harbor, ME). Homozygous *muMT* mice were provided by Prof. Chao Wang at Zhejiang University. Pax5flox/flox and CD19flox/flox mice were purchased from Cyagen Biosciences (Suzhou, China). C57BL/6 (CD45.2) mice were purchased from The Model Animal Research Center of Nanjing University (Nanjing, China). Mice at 6-12 weeks of age were used for animal experiments. For in situ mice model, a 20 μl suspension consisting of 50% Matrigel Basement Membrane Matrix (Corning, Teterboro, NJ) and 50% phosphate buffered saline (PBS; Cienry, Hangzhou, China) with Hepa1-6 cells in combination with macrophages were injected into the liver of mice. For syngeneic model, Hepa1-6 cells with 100 μl PBS were inoculated subcutaneously into the left or right flanks of mice. Sacrificed tumors were processed for further experiments.

Transfection of lentiviral vectors, siRNA and plasmid

THP-1 cells and iBMDMs were seeded in 6-well plates at a density of 2×10^5 cells/ml and infected with lenti-*PAX5*, lenti-*TFEB* or lenti-*NC* (Jikai, Shanghai, China). Stably transduced cells were purified using fluorescence activated cell sorting for further

experiments. For siRNA transfection, 1.5×10^5 per well THP-1 cells were seeded in 24-well plates and transfected with human *TFEB* siRNA (Santa Cruz Biotechnology, Santa Cruz, CA) using lipofectamine RNAimax (ThermoFisher Scientific, Waltham, MA) for 48 hours according to manufacturer's protocols. For plasmids transfection, HEK-293T cells were seeded in suitable density, the plasmids were transfected with Lipo8000™ Transfection Reagent (Beyotime, Shanghai, China) according to the manufacturer's instructions. After incubation for 24 h, the transfected cells were subjected to indicated analysis.

Targeted anti-CD19 CAR-T cell therapy

$CD19^+/CD19^-$ macrophages were isolated from the spleens of mice ($CD45^+CD11b^+F4/80^+CD19^+$), and were mixed with Hepa1-6 cells to establish subcutaneous xenograft model at the left ($CD19^+$ macrophages) or right ($CD19^-$ macrophages) flank of C57BL/6 or *muMT* mice. Anti-CD19 CAR-T cells were prepared and expanded. Mice were randomly assigned into groups for T cell infusion (1×10^7 cells in 100 μL PBS), and were sacrificed after 14 days. Harvested tumors were processed for subsequent experiments.

ImageStream analysis

Single-cell suspensions were stained and observed using an ImageStream II system (Amnis Corp, Seattle, WA) to identify CD19+ macrophages, CD19- macrophages, and B cells. Totally 1×10^5 single and focus cells were collected and analyzed by IDEASTM 6.2 software (Amnis Corp).

Multiplex immunohistochemistry (mIHC)

HCC and para-tumor were prepared into slides with 4-μm thickness. mIHC was performed using Opal™ 6-Plex Detection Kits (Akoya Biosciences, Marlborough, MA) according to the manufacturer's instructions.

Single-cell RNA sequencing (scRNA-seq) and RNA-seq

ScRNA-seq libraries were constructed using a Chromium Single Cell 3' Library and Gel Bead Kit v3.1 (10 x Genomics) according to the manufacturer's protocol. RNA-seq was performed using the Illumina Hiseq XTEN platform (Illumina, San Diego, CA, USA) at Novogene Co. Ltd (Beijing, China).

Statistical analysis

Statistical analysis was conducted using GraphPad Prism 8 (GraphPad Inc., La Jolla, CA).

Data availability

The remaining data are available within the Article, Supplementary Information or Source Data file. Source data are provided with this paper. Any additional information required to reanalyze the data reported in this paper is always available from the lead contact upon request (Qi Zhang: qi.zhang@zju.edu.cn). For external requests of additional data or materials required to reproduce the results presented in this manuscript, the requester must submit a formal application stating the research purpose, intended use of the data, and commitment to abide by relevant data protection and ethical guidelines.Human sequencing data were deposited in Genome Sequence Archive (GSA) (https://ngdc.cncb.ac.cn/gsa-human/browse/HRA008143). All processed sequencing data are deposited in Science Data Bank database, available via https://cstr.cn/31253.11.sciencedb.11557 or CSTR:31253.11.sciencedb.11557.

References

1. Sung H, Ferlay J, Siegel RL, Laversanne M, Soerjomataram I, Jemal A, Bray F. Global Cancer Statistics 2020: GLOBOCAN Estimates of Incidence and Mortality Worldwide for 36 Cancers in 185 Countries. *CA Cancer J Clin* **71**(3):209-249 (2021).

2. Forner A, Llovet JM, Bruix J. Hepatocellular carcinoma. *Lancet* **379**(9822):1245-1255 (2012).

3. Gordan JD, Kennedy EB, Abou-Alfa GK, Beg MS, Brower ST, Gade TP, Goff L, Gupta S, Guy J, Harris WP *et al*. Systemic Therapy for Advanced Hepatocellular Carcinoma: ASCO Guideline. *J Clin Oncol* **38**(36):4317-4345 (2020).

4. Vogel A, Meyer T, Sapisochin G, Salem R, Saborowski A. Hepatocellular carcinoma. *Lancet* **400**(10360):1345-1362 (2022).

5. Marra F, Tacke F. Roles for chemokines in liver disease. *Gastroenterology* **147**(3):577-594 (2014).

6. Zhang Q, Lou Y, Yang J, Wang J, Feng J, Zhao Y, Wang L, Huang X, Fu Q, Ye M *et al*. Integrated multiomic analysis reveals comprehensive tumour heterogeneity and novel immunophenotypic classification in hepatocellular carcinomas. *Gut* **68**(11):2019-2031 (2019).

7. Kalathil S, Lugade AA, Miller A, Iyer R, Thanavala Y. Higher frequencies of GARP(+)CTLA-4(+)Foxp3(+) T regulatory cells and myeloid-derived suppressor cells in hepatocellular carcinoma patients are associated with impaired T-cell functionality. *Cancer Res* **73**(8):2435-2444 (2013).

8. Shen KY, Zhu Y, Xie SZ, Qin LX. Immunosuppressive tumor microenvironment and immunotherapy of hepatocellular carcinoma: current status and prospectives. *J Hematol Oncol* **17**(1):25 (2024).

9. Noy R, Pollard JW. Tumor-associated macrophages: from mechanisms to therapy.

Immunity **41**(1):49-61 (2014).

10. Binnewies M, Roberts EW, Kersten K, Chan V, Fearon DF, Merad M, Coussens LM, Gabrilovich DI, Ostrand-Rosenberg S, Hedrick CC *et al*. Understanding the tumor immune microenvironment (TIME) for effective therapy. *Nat Med* **24**(5):541-550 (2018).
11. Murray PJ. Macrophage Polarization. *Annu Rev Physiol* **79**:541-566 (2017).
12. Mantovani A, Sozzani S, Locati M, Allavena P, Sica A. Macrophage polarization: tumor-associated macrophages as a paradigm for polarized M2 mononuclear phagocytes. *Trend Immunol* **23**(11):549-555 (2002).
13. DeNardo DG, Ruffell B. Macrophages as regulators of tumour immunity and immunotherapy. *Nat Rev Immunol* **19**(6):369-382 (2019).
14. Wu Q, Zhou W, Yin S, Zhou Y, Chen T, Qian J, Su R, Hong L, Lu H, Zhang F *et al*. Blocking triggering receptor expressed on myeloid cells-1-positive tumor-associated macrophages induced by hypoxia reverses immunosuppression and anti-programmed cell death ligand 1 resistance in liver cancer. *Hepatology* **70**(1):198-214 (2019).
15. Gordon SR, Maute RL, Dulken BW, Hutter G, George BM, McCracken MN, Gupta R, Tsai JM, Sinha R, Corey D *et al*. PD-1 expression by tumour-associated macrophages inhibits phagocytosis and tumour immunity. *Nature* **545**(7655):495-499 (2017).
16. Kim HJ, Park JH, Kim HC, Kim CW, Kang I, Lee HK. Blood monocyte-derived CD169(+) macrophages contribute to antitumor immunity against glioblastoma. *Nat Commun* **13**(1):6211 (2022).
17. Wang R, Li H, Ling C, Zhang X, Lu J, Luan W, Zhang J, Shi L. A novel phenotype of B cells associated with enhanced phagocytic capability and chemotactic function after ischemic stroke. *Neural Regen Res* **18**(11):2413-2423 (2023).

18. Kitamura D, Roes J, Kühn R, Rajewsky K. A B cell-deficient mouse by targeted disruption of the membrane exon of the immunoglobulin mu chain gene. *Nature* **350**(6317):423-426 (1991).

19. Allard B, Allard D, Buisseret L, Stagg J. The adenosine pathway in immuno-oncology. *Nat Rev Clin Oncol* **17**(10):611-629 (2020).

20. Junger WG. Immune cell regulation by autocrine purinergic signalling. *Nat Rev Immunol* **11**(3):201-212 (2011).

21. Antonioli L, Pacher P, Vizi ES, Haskó G. CD39 and CD73 in immunity and inflammation. *Trend Mol Med* **19**(6):355-367 (2013).

22. Zhang B .CD73: a novel target for cancer immunotherapy. *Cancer Res* **70**(16):6407-6411 (2010).

23. Vijayan D, Young A, Teng MWL, Smyth MJ. Targeting immunosuppressive adenosine in cancer. *Nat Rev Cancer* **17**(12):765 (2017).

24. Alcedo KP, Bowser JL, Snider NT. The elegant complexity of mammalian ecto-5'-nucleotidase (CD73). *Trend Cell Biol* **31**(10):829-842 (2021).

25. Depoil D, Fleire S, Treanor BL, Weber M, Harwood NE, Marchbank KL, Tybulewicz VL, Batista FD. CD19 is essential for B cell activation by promoting B cell receptor-antigen microcluster formation in response to membrane-bound ligand. *Nat Immunol* **9**(1):63-72 (2008).

26. Tedder TF.CD19: a promising B cell target for rheumatoid arthritis. *Nat Rev Rheumatol* **5**(10):572-577 (2009).

27. Chung EY, Psathas JN, Yu D, Li Y, Weiss MJ, Thomas-Tikhonenko A. CD19 is a major B cell receptor-independent activator of MYC-driven B-lymphomagenesis. *J Clin Invest* **122**(6):2257-2266 (2012).

28. Finck BN, Kelly DP. PGC-1 coactivators: inducible regulators of energy metabolism in health and disease. *J Clin Invest* **116**(3):615-622 (2006).

29. Cuervo AM, Mann L, Bonten EJ, d'Azzo A, Dice JF. Cathepsin A regulates chaperone-mediated autophagy through cleavage of the lysosomal receptor. *EMBO J* **22**(1):47-59 (2003).

30. Settembre C, Di Malta C, Polito VA, Garcia Arencibia M, Vetrini F, Erdin S, Erdin SU, Huynh T, Medina D, Colella P *et al*. TFEB links autophagy to lysosomal biogenesis. *Science* **332**(6036):1429-1433 (2011).

31. Roczniak-Ferguson A, Petit CS, Froehlich F, Qian S, Ky J, Angarola B, Walther TC, Ferguson SM. The transcription factor TFEB links mTORC1 signaling to transcriptional control of lysosome homeostasis. *Sci Signal* **5**(228):ra42 (2012).

32. Medina DL, Di Paola S, Peluso I, Armani A, De Stefani D, Venditti R, Montefusco S, Scotto-Rosato A, Prezioso C, Forrester A *et al*. Lysosomal calcium signalling regulates autophagy through calcineurin and TFEB. *Nat Cell Biol* **17**(3):288-299 (2015).

33. Van Rooijen N, Sanders A. Liposome mediated depletion of macrophages: mechanism of action, preparation of liposomes and applications. *J Immunol Method* **174**(1-2):83-93 (1994).

34. Moreno SG. Depleting Macrophages In Vivo with Clodronate-Liposomes. *Method Mol Biol* **1784**:259-262 (2018).

35. Xie H, Ye M, Feng R, Graf T. Stepwise reprogramming of B cells into macrophages. *Cell* **117**(5):663-676 (2004).

36. Chen C, Park B, Ragonnaud E, Bodogai M, Wang X, Zong L, Lee JM, Beerman I, Biragyn A. Cancer co-opts differentiation of B-cell precursors into macrophage-like cells. *Nat Commun* **13**(1):5376 (2022).

37. Hodawadekar S, Yu D, Cozma D, Freedman B, Sunyer O, Atchison ML, Thomas-Tikhonenko A. B-Lymphoma cells with epigenetic silencing of Pax5 trans-differentiate into macrophages, but not other hematopoietic lineages. *Exp Cell Res*

313(2):331-340 (2007).

38. Gabrilovich D. Myeloid-Derived Suppressor Cells. *Cancer Immunol Res* **5**(1): 3-8 (2017).
39. Veglia F, Sanseviero E, Gabrilovich D. Myeloid-derived suppressor cells in the era of increasing myeloid cell diversity. *Nat Rev Immunol* **21**(8):485–498 (2021).
40. Ma XL, Shen MN, Hu B, Wang BL, Yang WJ, Lv LH, Wang H, Zhou Y, Jin AL, Sun YF *et al*. CD73 promotes hepatocellular carcinoma progression and metastasis via activating PI3K/AKT signaling by inducing Rap1-mediated membrane localization of P110β and predicts poor prognosis. *J Hematol Oncol* **12**(1):37 (2019).
41. Supernat A, Markiewicz A, Welnicka-Jaskiewicz M, Seroczynska B, Skokowski J, Sejda A, Szade J, Czapiewski P, Biernat W, Zaczek A. CD73 expression as a potential marker of good prognosis in breast carcinoma. *App Immunohistochem Mol Morphol* **20**(2):103-107 (2012).
42. Beavis PA, Stagg J, Darcy PK, Smyth MJ. CD73: a potent suppressor of antitumor immune responses. *Trend Immunol* **33**(5):231-237 (2012).
43. Eichin D, Laurila JP, Jalkanen S, Salmi M. CD73 Activity is Dispensable for the Polarization of M2 Macrophages. *PloS One* **10**(8):e0134721 (2015).
44. Cappell KM, Kochenderfer JN. Long-term outcomes following CAR T cell therapy: what we know so far. *Nature reviews Clinical oncology* **20**(6):359-371 (2023).
45. The Lancet O . CAR T-cell therapy for solid tumours. *Lancet Oncol* **22**(7):893 (2021).
46. Albelda SM. CAR T cell therapy for patients with solid tumours: key lessons to learn and unlearn. *Nat Rev Clin Oncol* **21**(1):47-66 (2024).
47. Ashton TM, McKenna WG, Kunz-Schughart LA, Higgins GS. Oxidative phosphorylation as an emerging target in cancer therapy. *Clin Cancer Res* **24**(11):2482-2490 (2018).
48. Yap TA, Daver N, Mahendra M, Zhang J, Kamiya-Matsuoka C, Meric-Bernstam F,

Kantarjian HM, Ravandi F, Collins ME, Francesco MED *et al*. Complex I inhibitor of oxidative phosphorylation in advanced solid tumors and acute myeloid leukemia: phase I trials. *Nat Med* **29**(1):115-126 (2023).

Acknowledgements

This work was supported by National Key Research & Development Program (No. 2020YFA0804300), National Natural Science Foundation of China (Nos. 82071865, 82403723, 81871320, 32321002, 82188102, 92359304, 82403723), Zhejiang Provincial Natural Science Funds (Nos. LR20H160002, HDMD22H319373), Zhejiang Provincial Key Research & Development Program (No. 2021C03063), Zhejiang Provincial Medical and Health Technology Project (No. WKJ-ZJ-2403), and Zhejiang Provincial Traditional Chinese Medicine Science and Technology Project (No. GZY-ZJ-KJ-23025). We thank Jianfeng Wang from the Zhejiang Provincial Key Laboratory of Pancreatic Disease for sample collection. Dr. Qi Zhang also gratefully acknowledges the support of K.C.Wong Education Foundation.

Author contributions

T.L. and Q.Z. conceived the project. Q.Z., J.W. and J.S. designed the experiments. Q.Z., J.W., W.C., Y.Z., JQ.Y., JW.Y., J.T., M.Y., Z.H., J.W., H.D., and YQ.Z. performed most of the experiments under the supervision of T.L., X.B, X.L and P.X. R.Z., Y.L, X.L., and J.H. performed the bioinformatic analysis. Q.Z. and J.W. wrote the manuscript and the other authors made critical revisions.

Competing Interests statement

The authors declare no competing interests.

Corresponding authors

Correspondence to **Qi Zhang or Tingbo Liang.** Further information and requests for resources and reagents should be addressed to Qi Zhang (qi.zhang@zju.edu.cn).

Figure legends

Figure 1. CD19$^+$ macrophages are enriched in HCC (See also Figure S1).

(**A**) Visualized tSNE representation of the immune cell subtypes in human HCC tissues, including CD19$^+$ TAMs, CD19$^-$ TAMs, and B cells (left) and CD19 protein expression levels in these three clusters (right). Clusters are differently color-coded and annotated in the figure. Data were generated from CyTOF. (**B**) Representative immunofluorescence images of CD19$^+$ TAMs in HCC tissue and adjacent normal tissue. Scale bar, 50 μm. White arrows indicate CD19$^+$ TAMs. n = 191 independent experiments. (**C**) ImageStream showing CD19$^+$ TAMs, CD19$^-$ TAMs and B cells in HCC tissue at a single-cell level. ×40 magnification. (**D**) Representative flow cytometry plots showing CD19 expression on TAMs in HCC tissue, adjacent normal tissue, and peripheral blood. (**E**) Multiplex IHC assay was used to identify CD19$^+$ macrophages and B cells in formalin-fixed and paraffin-embedded HCC and adjacent normal tissues. Different colors indicate CD14 (yellow), CD68 (green), CD20 (orange), CD19 (red), and DAPI (blue). CD19$^+$ macrophages are identified as CD14$^+$CD68$^+$CD20$^-$CD19$^+$, whereas B cells are identified as CD14$^-$CD68$^-$CD20$^+$CD19$^+$. Scale bars, 50 μm. n = 20 independent experiments.(**F**) Flow cytometry quantification of CD19$^+$ TAMs proportion in different types of cancer. n = 28 (patients with hepatocellular carcinoma), n =11 (patients with renal cancer), n = 11 (patients with colorectal cancer), n = 13 (patients with pancreatic ductal adenocarcinoma), n = 12 (patients with breast cancer), n = 6 (patients with gastric cancer). Data are presented as the mean ± SEM. A paired two-tailed *t*-test was used in **F**.

Figure 2. $CD19^+$ TAMs are associated with poor clinical outcome and immunotherapy response (See also Figure S2 and S3).

(**A**) Kaplan-Meier curves showing overall survival of HCC patients with a high (> median) or low (< median) ratio of $CD19^+$ TAMs. Data are derived from immunofluorescence co-staining of human HCC tissue microarray. n = 149. (**B**) Kaplan-Meier curves show overall survival of HCC patients with a high or low TAMs ratio. Data are derived from immunofluorescence co-staining of human HCC tissue microarray. n = 149. (**C**) Correlation analysis between Ki-67^+ cells and $CD19^+$ TAMs density in HCC tissues. Data are derived from immunofluorescence co-staining of human HCC tissue microarray. n = 156. Scale bar, 50 μm; 100 μm. (**D**) Splenic $CD19^+$ and $CD19^-$ macrophages were sorted and separately mixed with 5×10^5 Hepa1-6 cells at the ratio of 1:5, and then injected into the liver of mice. Images and weight of the tumors were showed at 14 days post-inoculation. n = 5 per group. Tumors are indicated by red circles. (**E**) Splenic $CD19^+$ macrophages and $CD19^-$ macrophages were separately mixed with 5×10^5 Hepa1-6 cells at the ratio of 1:5, and then inoculated subcutaneously (*s.c.*) into mice. When tumors reached 35 to 45 mm^2, mice were received intravenous injection (*i.v.*) with GFP^+ control CAR-T cells or GFP^+ anti-CD19 CAR-T cells (1×10^7 cells in 100 μL of PBS). The harvested tumors were analyzed. n = 5 per group. (**F**) Splenic $CD19^+$ macrophages and $CD19^-$ macrophages were mixed with 5×10^5 Hepa1-6 cells at the ratio of 1:5, and then inoculated subcutaneously in the left and right flanks of *muMT* (lacking mature B cells) or wild-type (WT) mice. When tumors reached 35 to 45 mm^2, mice were received intravenous injection with GFP^+ control CAR-T cells or GFP^+ anti-CD19 CAR-T cells (1×10^7 cells in 100 μL of PBS). The harvested tumors were analyzed. n = 5 per group. Data are presented as the mean ± SEM. Log-rank test (**A, B**), Pearson correlation using a two-sided test (**C**), unpaired two-tailed *t*-test (**D, E**), or paired two-tailed *t* test (**F**) were used for statistical analysis. NS, not significant.

Figure 3. CD19$^+$ TAMs display a distinct gene expression profile (See also Figure S4, S5 and S6).

(**A**) Schematic diagram of scRNA-seq experimental strategy for human HCC tissues. n = 3. (**B**) UMAP plot analysis showing HCC samples (top panel) and cell types in the samples (bottom) as indicated. (**C**) Heatmap showing the top 10 upregulated genes in CD19$^+$ TAMs, CD19$^-$ TAMs and B cells, respectively. (**D**) mRNA expression levels of classical M1 and M2 macrophage marker genes in CD19$^+$ TAMs, compared with CD19$^-$ TAMs. Bubble size and color represent the percentages and relative levels, respectively, of upregulated or downregulated genes as indicated at the x axis. (**E**) Bar chart showing the top-ranked biological pathways in CD19$^+$ TAMs from KEGG enrichment analysis of the scRNA-seq data in (**A**). (**F**) t-SNE plots showing the expression levels of mitochondrion-related genes in CD19$^+$ and CD19$^-$ TAMs. (**G**) Violin plot analysis of mitochondrion-related gene expression levels in CD19$^+$ and CD19$^-$ TAMs. Data are mean ± SEM; An unpaired two-tailed *t*-test was used in (**G**).

Figure 4. CD19$^+$ TAMs are highly proliferative and immunosuppressive (See also Figure S7).

(**A**) Relative expression levels of mitochondrial metabolism-related genes in CD19$^+$ TAMs and CD19$^-$ TAMs in human HCC tissue. n = 3 independent experiments. (**B**) Mitochondrial OCR measurement in CD19$^+$ TAMs and CD19$^-$ TAMs (5×10^5 cells per well). n = 3 independent experiments. (**C**) Flow cytometry histograms and quantification showing the phagocytic ability in CD19$^+$ TAMs and CD19$^-$ TAMs. n = 3 independent experiments. (**D**) Flow cytometry histograms and quantification showing the levels of PD-L1 and CD73 in CD19$^+$ TAMs and CD19$^-$ TAMs. n = 5 independent experiments. (**E**) Normalized 5'-nucleotidase (CD73) specific activity of CD19$^+$ TAMs and CD19$^-$ TAMs lysate. n = 3 independent experiments. (**F**) Co-culture of CD19$^+$ TAMs or CD19$^-$ TAMs with CD3$^+$ T, CD4$^+$ T, CD8$^+$ T cells at different ratios for 72 h. n = 3 independent experiments. Data are mean ± SEM.; Unpaired two-tailed *t*-test (**B**, **E**), paired two-tailed *t* test (**C**, **D**), or two-way ANOVA test (**F**) were used.

Figure 5. PAX5 is a master regulator for CD19^{+} macrophages (See also Figure S8).

(**A**) Tumor images and weights of orthotopic HCC model in *CD19$^{\triangle M\varphi}$* (*CD19$^{flox/flox}$;Lyz-Cre*) and littermate wildtype mice. n = 4 per group. (**B**) Representative flow cytometrical images and quantification showing the proportion of CD19^{+} TAMs in the tumors from (**A**). (**C**) *PAX5* mRNA expression level in CD19^{+} TAMs and CD19^{-} TAMs. n = 6975 per group. (**D**) Flow cytometry histograms and quantification showing protein expression levels of PAX5 in CD19^{+} TAMs and CD19^{-} TAMs. n = 5 independent experiments. (**E**) Western blotting analysis of PAX5 expression level in CD19^{+} TAMs and CD19^{-} TAMs. Relative PAX5 blot intensities were shown. (**F**) Representative flow cytometry histograms showing the levels CD19, PD-L1, and CD73 in THP-1 cells with or without *PAX5* overexpression. (**G**) Western blotting analysis of CD19, PD-L1, and CD73 levels in THP-1 cells with or without *PAX5* overexpression. (**H**) Representative flow cytometry histograms showing the levels of CD19, PD-L1, and CD73 in iBMDM with or without *Pax5* overexpression. (**I**) Mitochondrial OCR measurement in THP-1 cells with or without *PAX5* overexpression (5× 10^5 cells per well). n = 3 independent experiments. (**J**) Electron microscopy images and quantification showing mitochondrias in THP-1 cells with or without *PAX5* overexpression. scale bar: 0.5 μm or 0.2 μm. n = 5 independent experiments. (**K**) Representative flow cytometry histograms showing mitochondrial number (mitotracker), and mitochondrial ROS level (MitoSOX) in THP-1 cells with or without *PAX5* overexpression. (**L**) Tumor images and sizes of orthotopic HCC model in *Pax5$^{\triangle M\varphi}$* (*Pax59$^{flox/flox}$;Lyz-Cre*) and littermate control mice. n= 5 per group. Representative image is shown n = 3 independent experiments in E and G. Data are mean ± SEM; One-way ANOVA with Welch's correction (**A**), unpaired two-tailed *t*-test (**B,I, J, L**), or paired two-tailed *t* test (**C, D**) were used. NS, not significant.

Figure 6. PAX5 induces PD-L1 and CD73 in a post-transcriptional manner (See also Figure S9).

(**A**) mRNA expression levels of *CD73,* and *PD-L1* in THP-1 cells with or without *PAX5* overexpression. n = 3 independent experiments. (**B**) Venn diagram showing the number and percentage of share genes in Cut&Tag and RNA-seq analyses of THP-1 cells with *PAX5* overexpression. (**C**) WebGestalt analysis of enriched biological pathways in the shared genes in (**B**). (**D**) KFERQ finder V0.8 identified KFERQ-like motifs in PD-L1 and CD73. (**E**) Immunoprecipitation (IP) of HSC70 followed by immunoblotting (IB) analyses for HSC70, PD-L1, and CD73 in THP-1 cells with or without *PAX5* overexpression. (**F**) Representative immunofluorescence images and quantification of Lysotracker (red) in THP-1 cells with or without *PAX5* overexpression or not. Blue color indicates DAPI staining; scale bar, 25 μm. n = 3 independent experiments. (**G**) Representative flow cytometry histograms and quantification showing the lysosome quantity assessed by LysoSensor fluorescence expression in THP-1 cells with or without *PAX5* overexpression. n = 3 independent experiments. (**H**) Western blotting detection of PD-L1 and CD73 in THP-1 cells with *PAX5* overexpression, or treated with inhibitors of lysosomal proteolysis (NH_4Cl, 20mM and leupeptin, 100μM), or inhibitor of proteasome (MG132, 5μM). LC3B is used as a marker of lysosomal proteolysis inhibition. (**I**) Western blotting detection of cytosol and nuclear TFEB in THP-1 cells with or without *PAX5* overexpression. (**J**) Fluorescent probe indicates relative Ca^{2+} levels in mitochondria (Rhod2) and cytoplasm (Calbryte^{TM} 630^{AM}) in THP-1 cells with or without *PAX5* overexpression. Fluorescence was measured every 30s for 30 minutes. n = 3 repeats. Representative image is shown n = 3 independent experiments in E, H and I. Data are mean ± SEM; An unpaired two-tailed *t*-test (**A, F, G**), or two-way ANOVA test (**J**) were used. NS, not significant.

Figure 7. Blocking CD19$^+$ TAMs enhances the efficacy of immune checkpoint blockade therapy (See also Figures S10, S11, and S12).

(**A**) Hepa1-6 cells (5× 10^5) were mixed with iBMDMs (with or without *Pax5* overexpression) at a ratio of 1:1, and orthotopically injected into the livers of C57BL/6 mice. Tumor images and sizes were showed at 15 days post-inoculation. Tumor sites were indicated by red dotted line in liver. Upper panel: tumors in situ (attached to liver tissue). Lower panel: The same tumors after complete dissection from the liver. n = 5 per group. (**B**) Representative immunohistochemistrical images and quantification showing the infiltrated CD8$^+$ T cells in the tumors of (**A**). Scale bar, 50 μm. n = 4 per group.(**C**) Schematic diagram illustrating targeted therapy of CD73 and PD-L1 for CD19$^+$ TAMs in HCC. Tumors were established by inoculating 5× 10^5 Hepa1-6 cells and iBMDMs with *Pax5* overexpression at the ratio of 1:1. Seven days post-inoculation, mice were treated as indicated. i.p, intraperitoneal injections; i.g, oral gavage. (**D**) Tumor images and sizes of (**C**). n = 5 per group. Tumor sites were indicated by red dotted line in the liver. (**E**) Tumor images and sizes in the in vivo experiment targeting OXPHOS and PD-L1 in CD19$^+$ TAM. Tumors were established by inoculating 5× 10^5 Hepa1-6 cells and iBMDMs with *Pax5* overexpression at the ratio of 1:1. Seven days post-inoculation, mice were treated as indicated. n = 5 per group. Tumor sites were indicated by red line in the liver. Data are mean ± SEM; Unpaired two-tailed *t*-test (**A, B**), or unpaired one-way ANOVA with Welch's correction (**D, E**) were used.

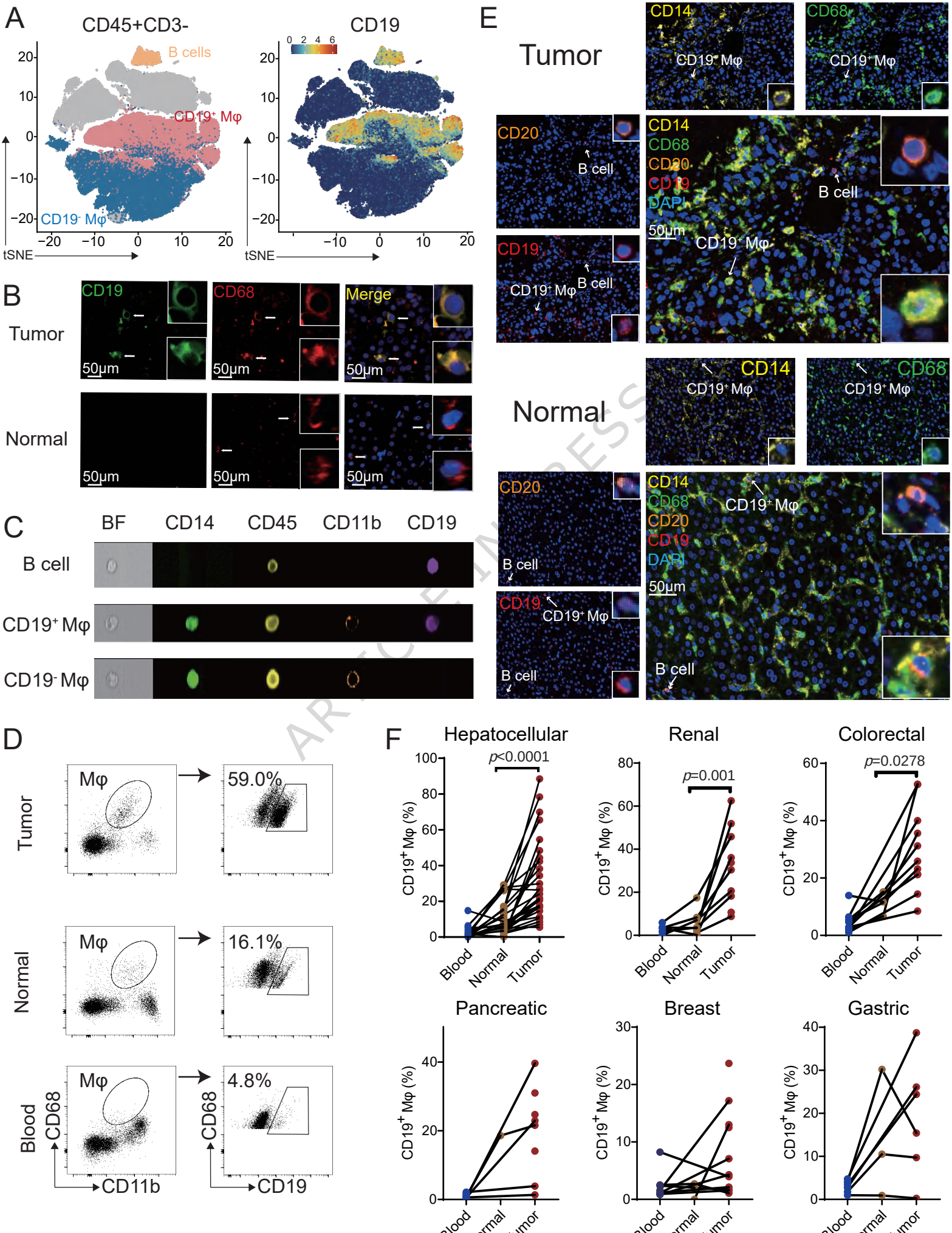
A
CD45+CD3-
B cells
CD19+ Mφ
CD19- Mφ
tSNE
CD19
0 2 4 6
tSNE
B
Tumor
Normal
CD19
CD68
Merge
50μm
C
BF
CD14
CD45
CD11b
CD19
B cell
CD19+ Mφ
CD19- Mφ
D
Tumor
Normal
Blood
Mφ
59.0%
16.1%
4.8%
CD68
CD11b
CD19
E
Tumor
Normal
CD14
CD68
CD20
CD19
DAPI
B cell
CD19+ Mφ
50μm
F
Hepatocellular
Renal
Colorectal
Pancreatic
Breast
Gastric
p<0.0001
p=0.001
p=0.0278
CD19+ Mφ (%)
Blood
Normal
Tumor

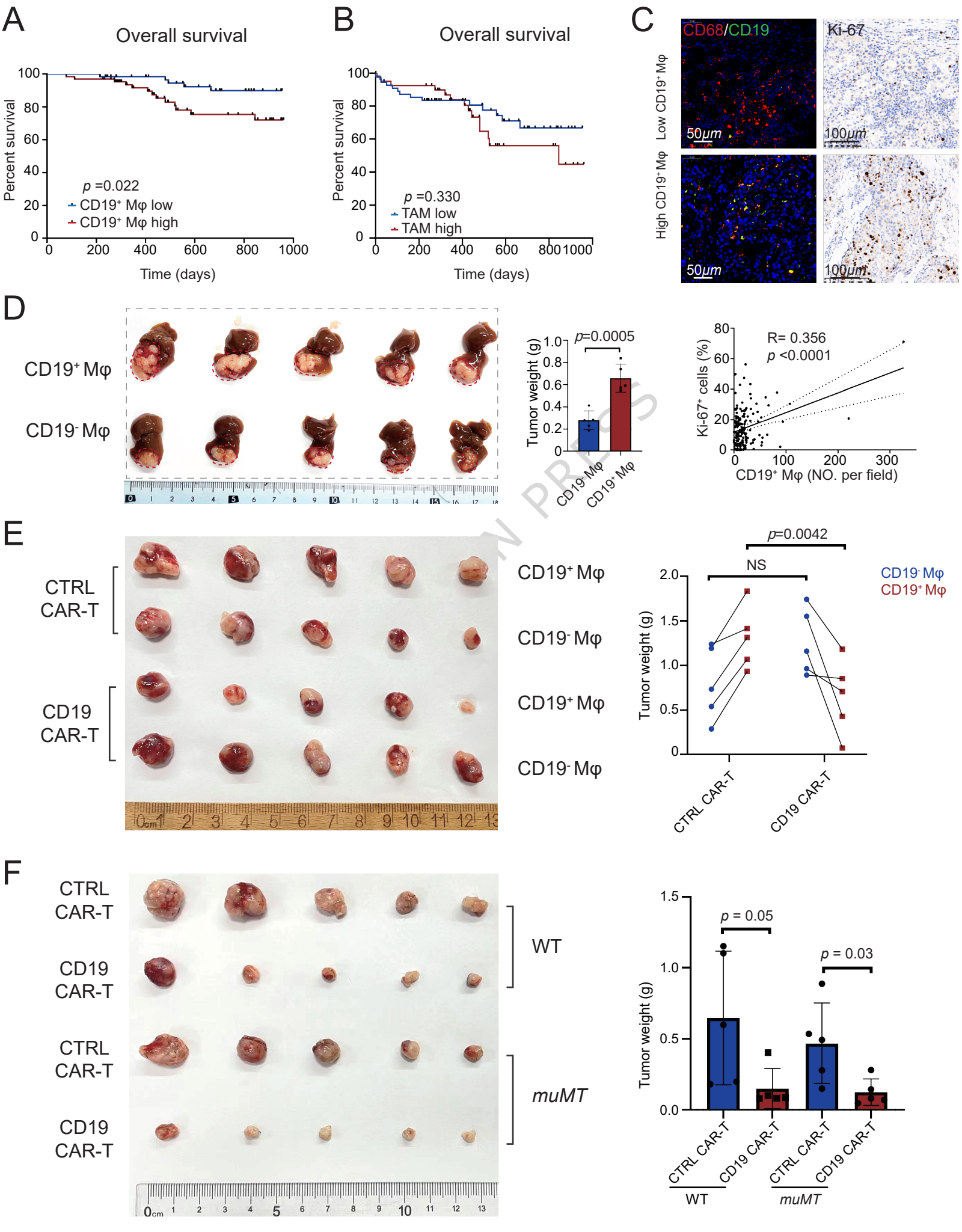
A
Overall survival
Percent survival
Time (days)
p =0.022
CD19⁺ Mφ low
CD19⁺ Mφ high
B
Overall survival
Percent survival
Time (days)
p =0.330
TAM low
TAM high
C
CD68/CD19
Ki-67
Low CD19⁺ Mφ
High CD19⁺ Mφ
50μm
100μm
D
CD19⁺ Mφ
CD19⁻ Mφ
Tumor weight (g)
p=0.0005
CD19⁻ Mφ
CD19⁺ Mφ
Ki-67⁺ cells (%)
R= 0.356
p <0.0001
CD19⁺ Mφ (NO. per field)
E
CTRL CAR-T
CD19 CAR-T
CD19⁺ Mφ
CD19⁻ Mφ
CD19⁺ Mφ
CD19⁻ Mφ
p=0.0042
NS
CD19⁻ Mφ
CD19⁺ Mφ
Tumor weight (g)
CTRL CAR-T
CD19 CAR-T
F
CTRL CAR-T
CD19 CAR-T
CTRL CAR-T
CD19 CAR-T
WT
muMT
Tumor weight (g)
p = 0.05
p = 0.03
CTRL CAR-T
CD19 CAR-T
CTRL CAR-T
CD19 CAR-T
WT
muMT

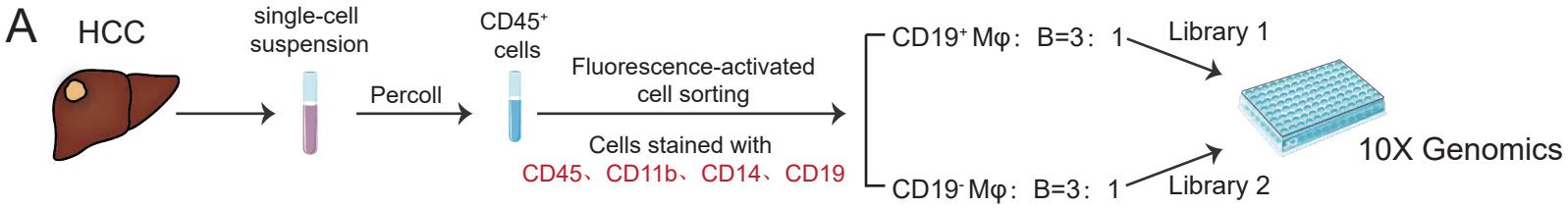
A
HCC
single-cell suspension
Percoll
CD45+ cells
Fluorescence-activated cell sorting
Cells stained with
CD45、CD11b、CD14、CD19
CD19+ Mφ: B=3: 1
CD19- Mφ: B=3: 1
Library 1
Library 2
10X Genomics

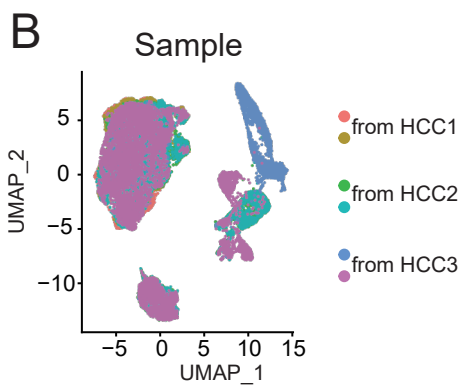
B
Sample
from HCC1
from HCC2
from HCC3
UMAP_2
UMAP_1

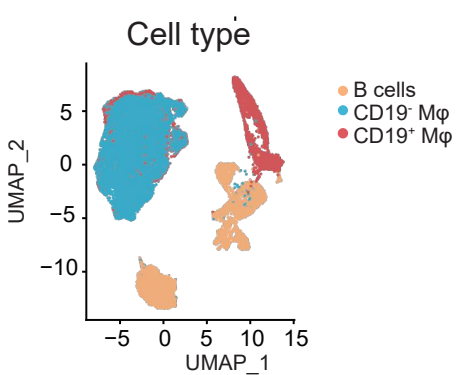
Cell type
B cells
CD19- Mφ
CD19+ Mφ
UMAP_2
UMAP_1

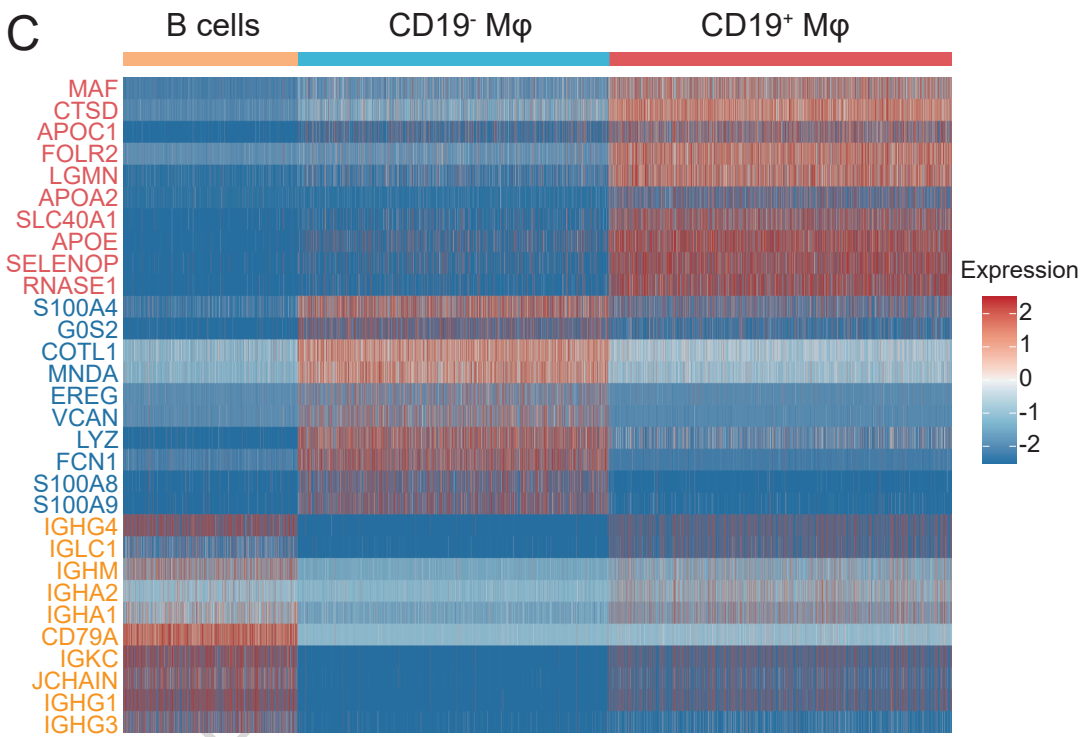
C
B cells
CD19- Mφ
CD19+ Mφ
MAF
CTSD
APOC1
FOLR2
LGMN
APOA2
SLC40A1
APOE
SELENOP
RNASE1
S100A4
G0S2
COTL1
MNDA
EREG
VCAN
LYZ
FCN1
S100A8
S100A9
IGHG4
IGLC1
IGHM
IGHA2
IGHA1
CD79A
IGKC
JCHAIN
IGHG1
IGHG3
Expression

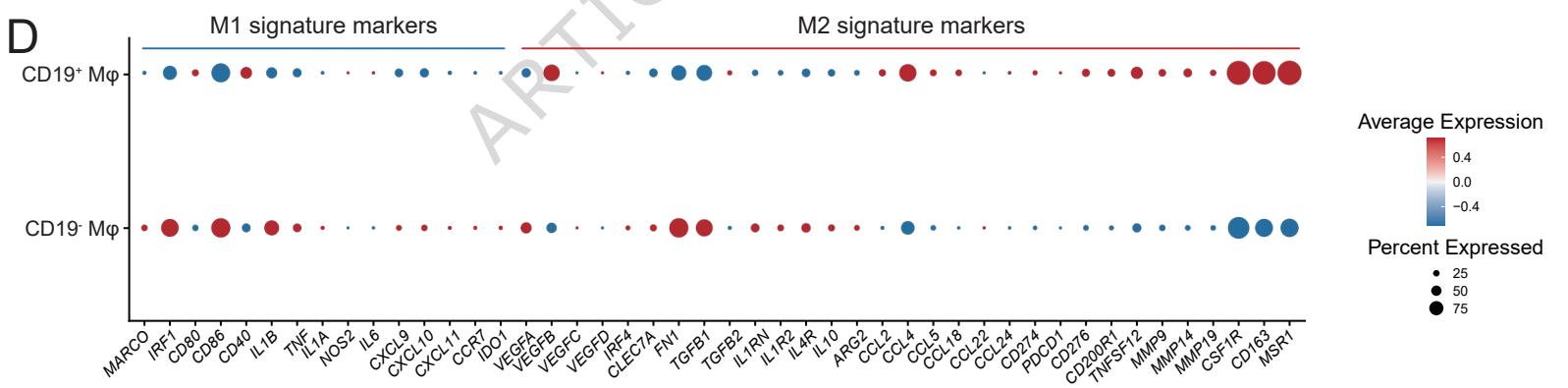
D
M1 signature markers
M2 signature markers
CD19+ Mφ
CD19- Mφ
MARCO IRF1 CD80 CD86 CD40 IL1B TNF IL1A NOS2 IL6 CXCL9 CXCL10 CXCL11 CCR7 IDO1 VEGFA VEGFB VEGFC VEGFD IRF4 CLEC7A FN1 TGFB1 TGFB2 IL1RN IL1R2 IL4R IL10 ARG2 CCL2 CCL4 CCL5 CCL18 CCL22 CCL24 CD274 PDCD1 CD276 CD200R1 TNFSF12 MMP9 MMP14 MMP19 CSF1R CD163 MSR1
Average Expression
Percent Expressed

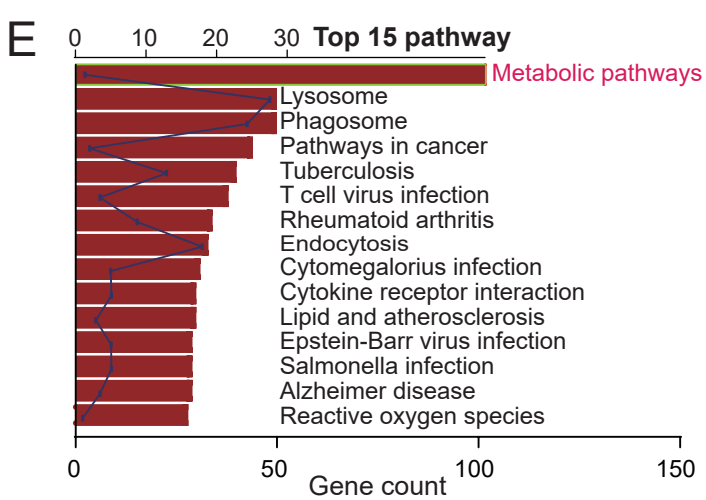
E
Top 15 pathway
Metabolic pathways
Lysosome
Phagosome
Pathways in cancer
Tuberculosis
T cell virus infection
Rheumatoid arthritis
Endocytosis
Cytomegalorius infection
Cytokine receptor interaction
Lipid and atherosclerosis
Epstein-Barr virus infection
Salmonella infection
Alzheimer disease
Reactive oxygen species
Gene count

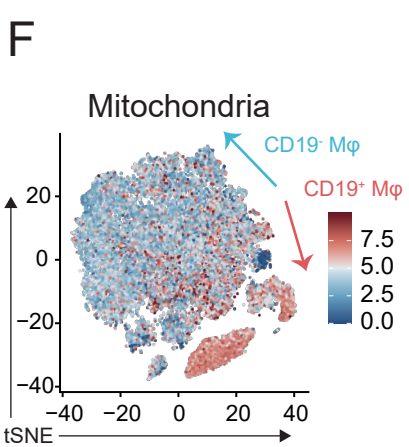
F
Mitochondria
CD19- Mφ
CD19+ Mφ
tSNE

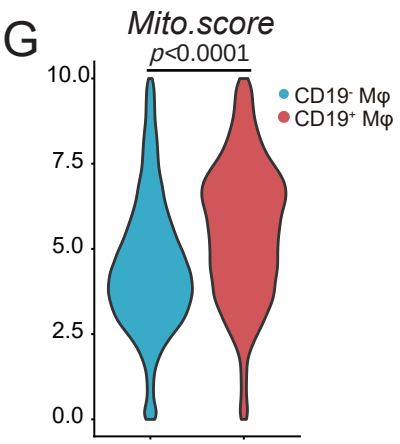
G
Mito.score
p<0.0001
CD19- Mφ
CD19+ Mφ

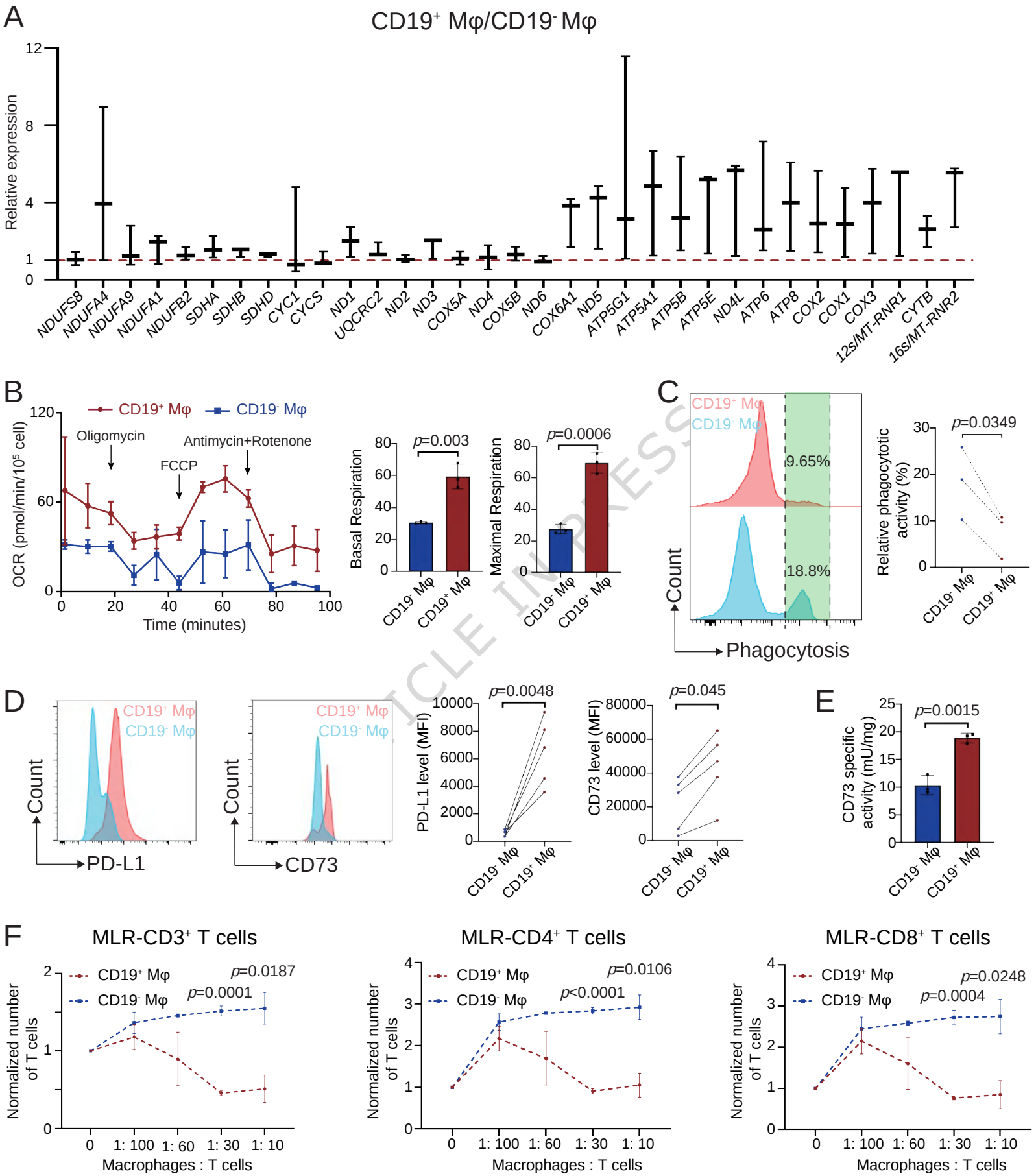
A
CD19+ Mφ/CD19- Mφ
Relative expression
12
8
4
1
0
NDUFS8
NDUFA4
NDUFA9
NDUFA1
NDUFB2
SDHA
SDHB
SDHD
CYC1
CYCS
ND1
UQCRC2
ND2
ND3
COX5A
ND4
COX5B
ND6
COX6A1
ND5
ATP5G1
ATP5A1
ATP5B
ATP5E
ND4L
ATP6
ATP8
COX2
COX1
COX3
12s/MT-RNR1
CYTB
16s/MT-RNR2
B
CD19+ Mφ
CD19- Mφ
OCR (pmol/min/10^5 cell)
Oligomycin
FCCP
Antimycin+Rotenone
Time (minutes)
Basal Respiration
p=0.003
Maximal Respiration
p=0.0006
C
CD19+ Mφ
CD19- Mφ
9.65%
18.8%
Count
Phagocytosis
Relative phagocytic activity (%)
p=0.0349
D
CD19+ Mφ
CD19- Mφ
Count
PD-L1
CD73
PD-L1 level (MFI)
p=0.0048
CD73 level (MFI)
p=0.045
E
CD73 specific activity (mU/mg)
p=0.0015
F
MLR-CD3+ T cells
MLR-CD4+ T cells
MLR-CD8+ T cells
Normalized number of T cells
p=0.0187
p=0.0001
p=0.0106
p<0.0001
p=0.0248
p=0.0004
0
1: 100
1: 60
1: 30
1: 10
Macrophages : T cells

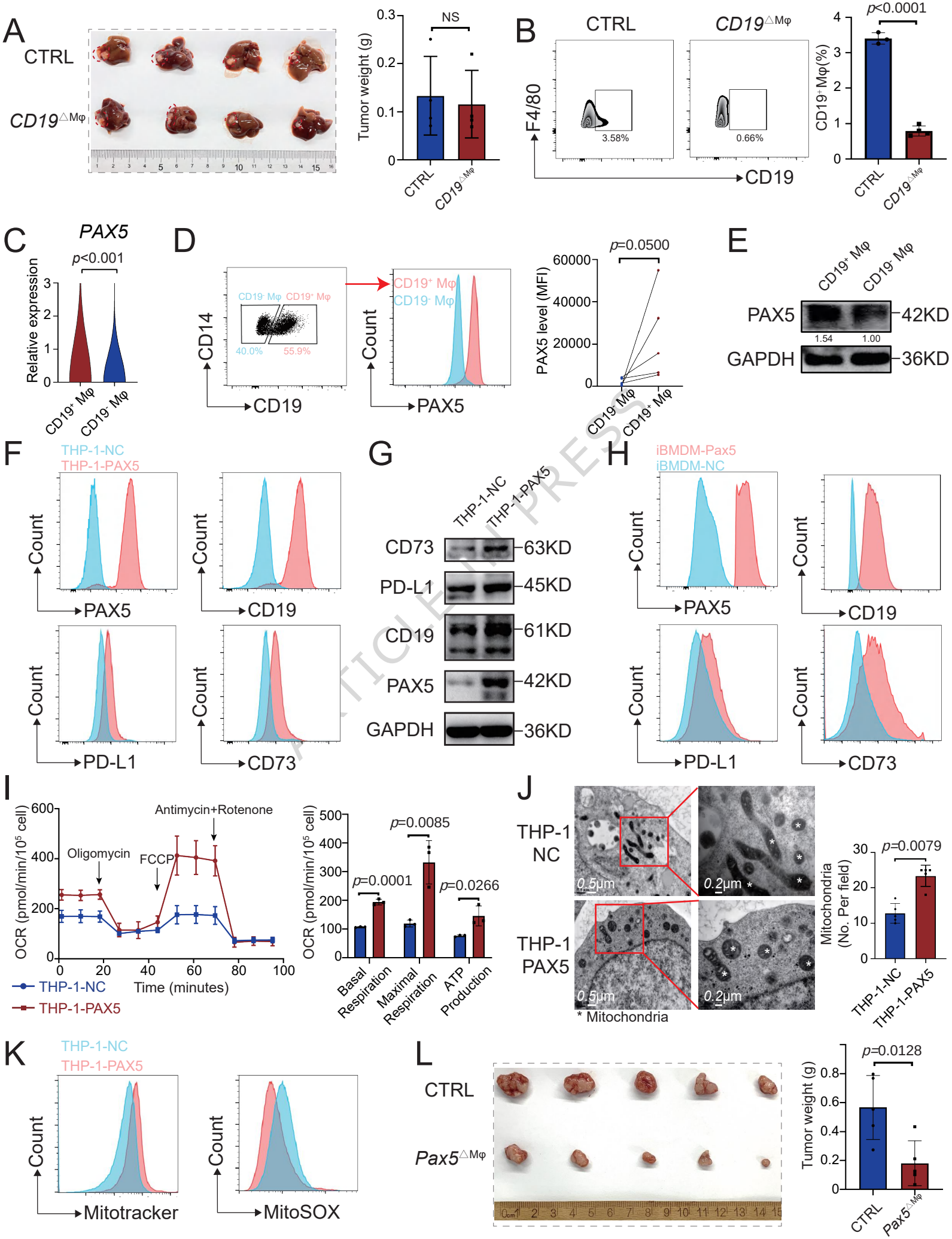
A
CTRL
CD19△Mφ
Tumor weight (g)
NS
B
CTRL
CD19△Mφ
F4/80
CD19
3.58%
0.66%
CD19⁺ Mφ(%)
p<0.0001
C
PAX5
p<0.001
Relative expression
CD19⁺ Mφ
CD19⁻ Mφ
D
CD19⁻ Mφ CD19⁺ Mφ
40.0%
55.9%
CD14
CD19
Count
PAX5
p=0.0500
PAX5 level (MFI)
E
CD19⁺ Mφ
CD19⁻ Mφ
PAX5
42KD
1.54
1.00
GAPDH
36KD
F
THP-1-NC
THP-1-PAX5
Count
PAX5
CD19
PD-L1
CD73
G
THP-1-NC
THP-1-PAX5
CD73
63KD
PD-L1
45KD
CD19
61KD
PAX5
42KD
GAPDH
36KD
H
iBMDM-Pax5
iBMDM-NC
Count
PAX5
CD19
PD-L1
CD73
I
OCR (pmol/min/10⁵ cell)
Oligomycin
FCCP
Antimycin+Rotenone
Time (minutes)
THP-1-NC
THP-1-PAX5
p=0.0001
p=0.0085
p=0.0266
Basal Respiration
Maximal Respiration
ATP Production
J
THP-1 NC
THP-1 PAX5
0.5μm
0.2μm
* Mitochondria
Mitochondria (No. Per field)
p=0.0079
K
THP-1-NC
THP-1-PAX5
Count
Mitotracker
MitoSOX
L
CTRL
Pax5△Mφ
Tumor weight (g)
p=0.0128

A

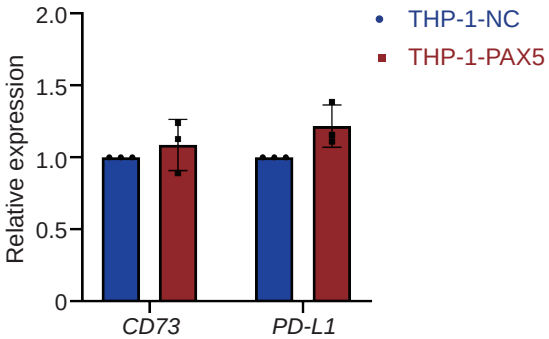

C

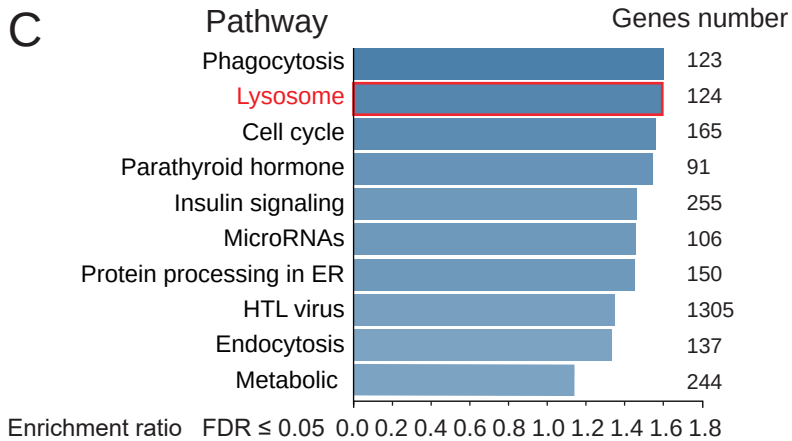

B

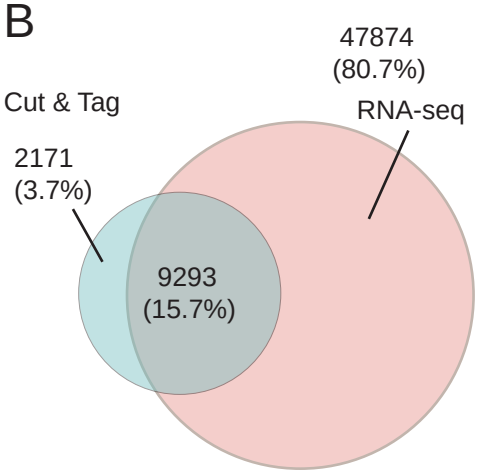

D

KFERQ Finder

protein name	PD-L1	CD73
UniProt ID	Q9NZQ7	P21589
motif	DLKVQ LLKDQ DVKLQ	FTKVQ VDKLK DRVVK
motif_type	canonical canonical canonical	phos.act. acetyl.act. acetyl.act.

E

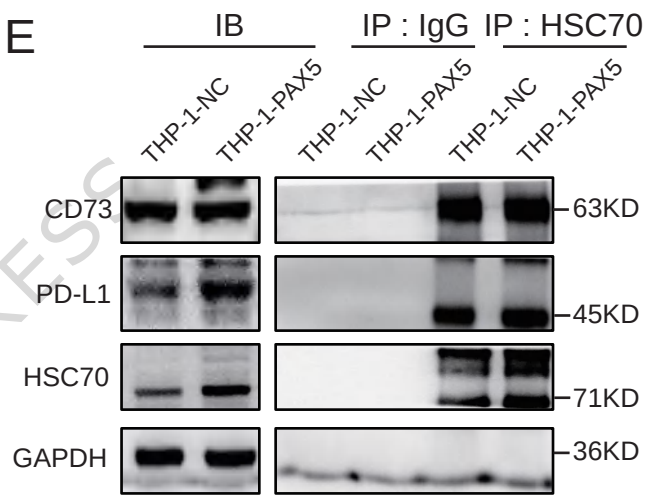

F

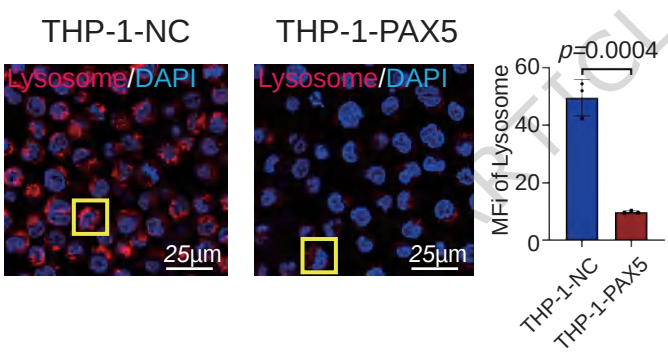

G

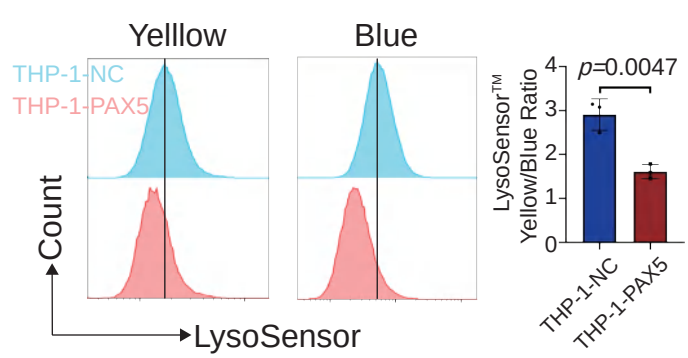

H

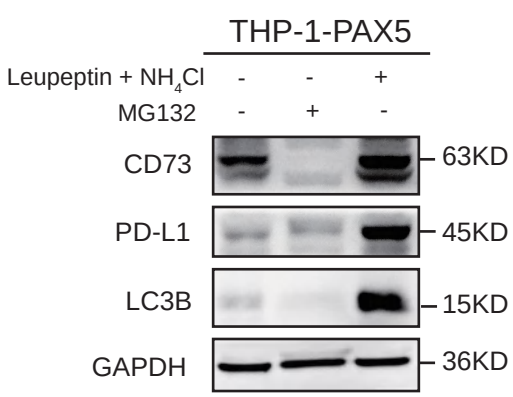

I

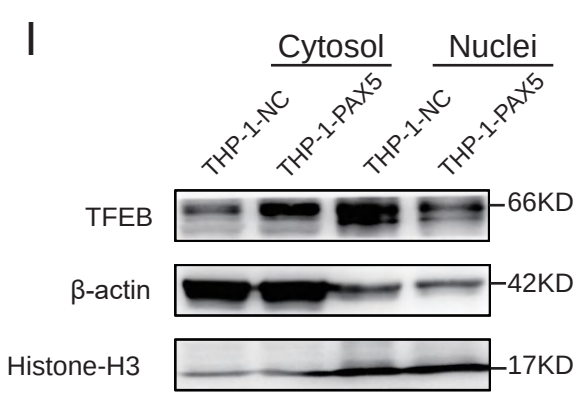

J

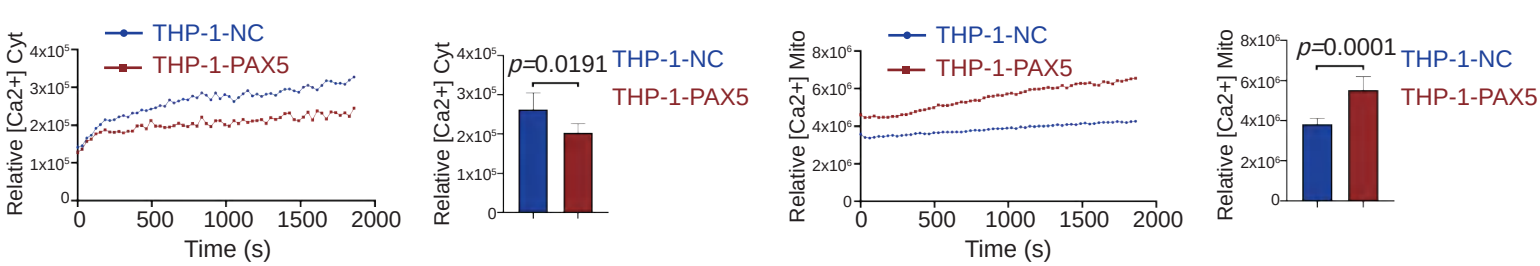

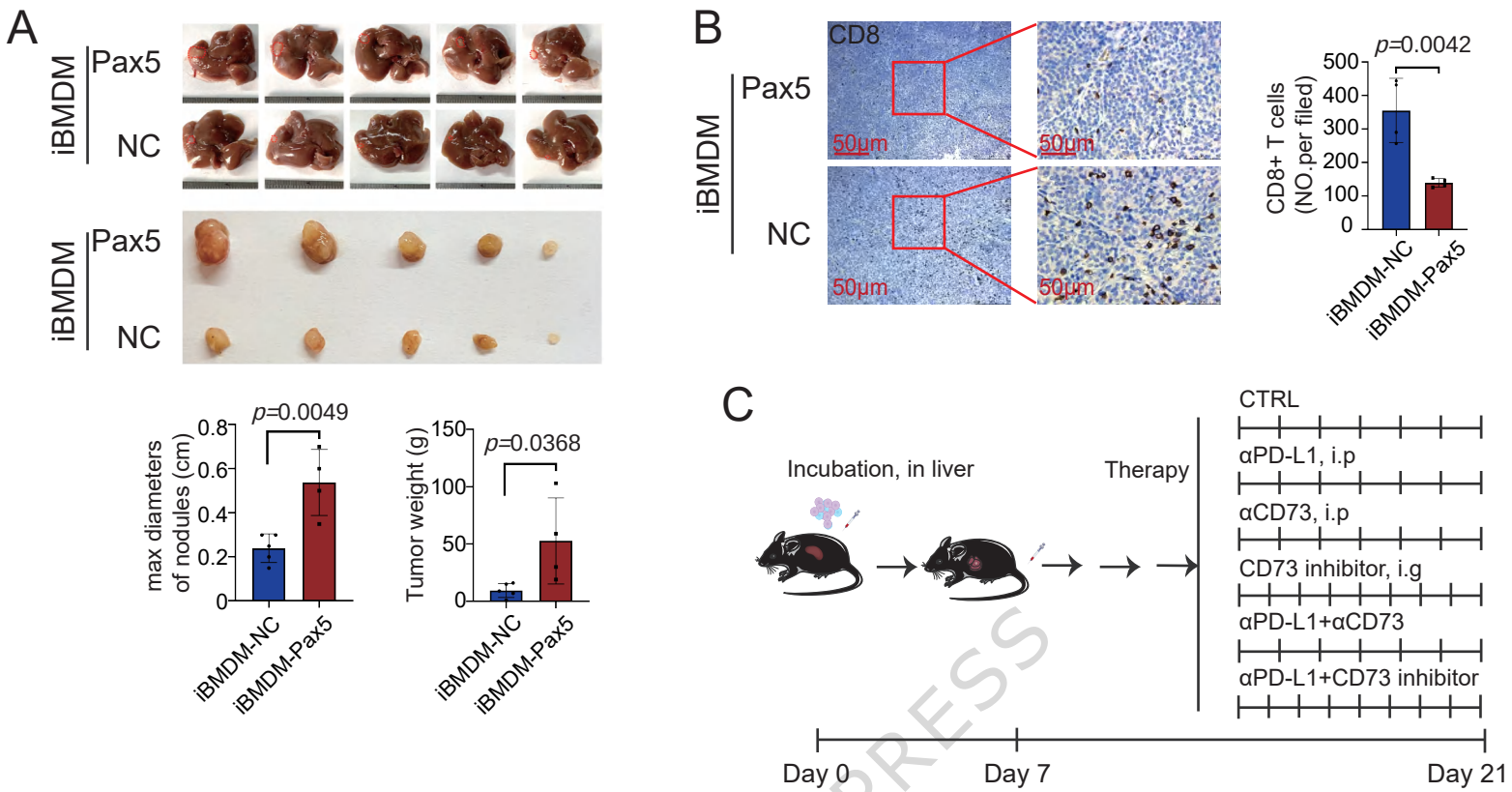
A
iBMDM
Pax5
NC
iBMDM
Pax5
NC
max diameters of nodules (cm)
p=0.0049
iBMDM-NC
iBMDM-Pax5
Tumor weight (g)
p=0.0368
iBMDM-NC
iBMDM-Pax5
B
iBMDM
Pax5
NC
CD8
50μm
50μm
50μm
50μm
CD8+ T cells (NO.per filed)
p=0.0042
iBMDM-NC
iBMDM-Pax5
C
Incubation, in liver
Therapy
CTRL
αPD-L1, i.p
αCD73, i.p
CD73 inhibitor, i.g
αPD-L1+αCD73
αPD-L1+CD73 inhibitor
Day 0
Day 7
Day 21

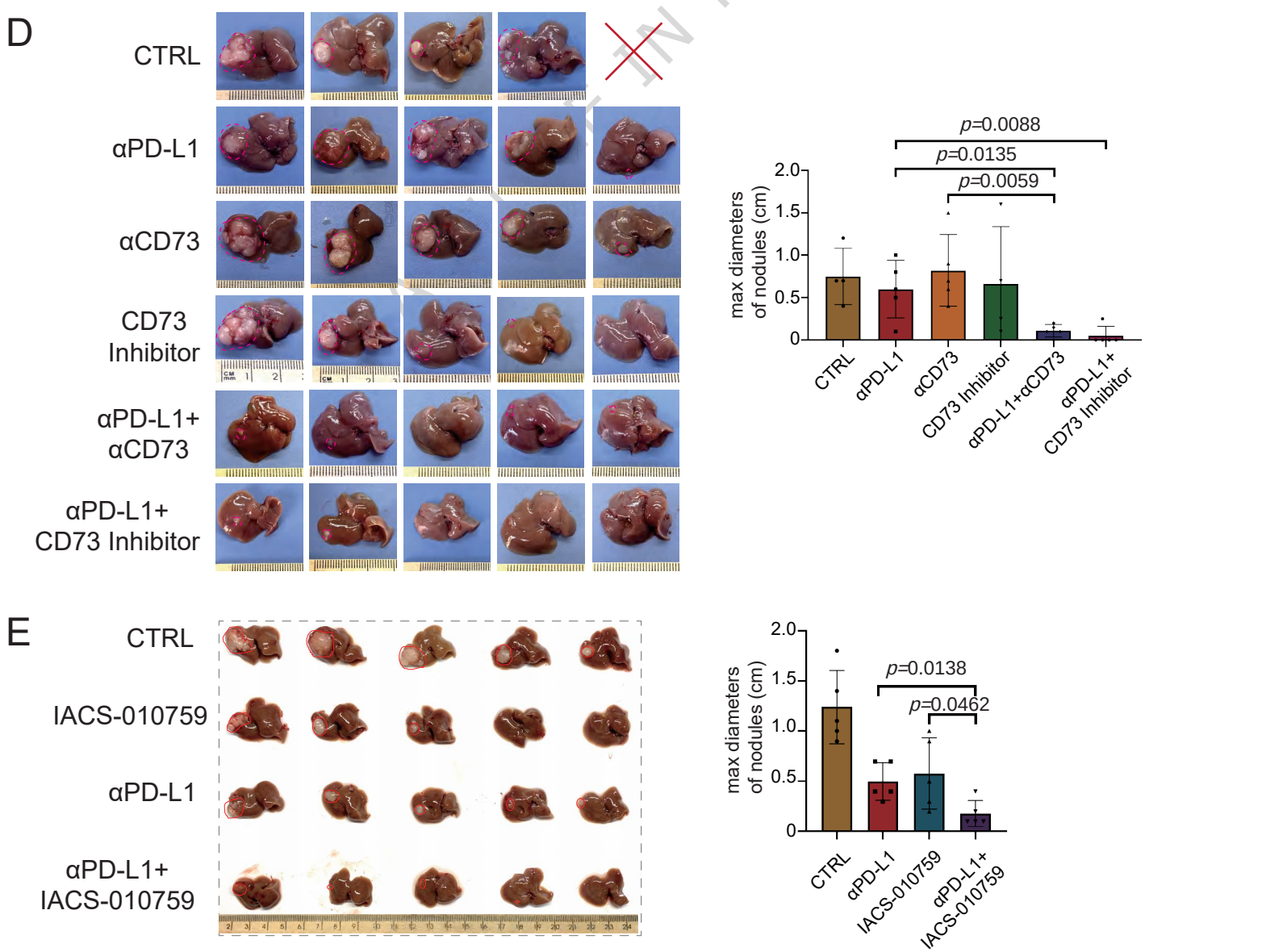
D
CTRL
αPD-L1
αCD73
CD73 Inhibitor
αPD-L1+ αCD73
αPD-L1+ CD73 Inhibitor
p=0.0088
p=0.0135
p=0.0059
max diameters of nodules (cm)
CTRL
αPD-L1
αCD73
CD73 Inhibitor
αPD-L1+αCD73
αPD-L1+ CD73 Inhibitor
E
CTRL
IACS-010759
αPD-L1
αPD-L1+ IACS-010759
p=0.0138
p=0.0462
max diameters of nodules (cm)
CTRL
αPD-L1
IACS-010759
αPD-L1+ IACS-010759